Accepted Manuscript

Active vibration control of smart composite plates using optimized self-tuning fuzzy logic controller with optimization of placement, sizing and orientation of PFRC actuators

Nemanja D. Zorić, Aleksandar M. Tomović, Aleksandar M. Obradović, Radoslav D. Radulović, Goran R. Petrović

PII: S0022-460X(19)30304-9

DOI: https://doi.org/10.1016/j.jsv.2019.05.035

Reference: YJSVI 14772

To appear in: *Journal of Sound and Vibration*

Received Date: 22 December 2018

Revised Date: 30 April 2019

Accepted Date: 15 May 2019

Please cite this article as: N.D. Zorić, A.M. Tomović, A.M. Obradović, R.D. Radulović, G.R. Petrović, Active vibration control of smart composite plates using optimized self-tuning fuzzy logic controller with optimization of placement, sizing and orientation of PFRC actuators, *Journal of Sound and Vibration* (2019), doi: https://doi.org/10.1016/j.jsv.2019.05.035.

Active vibration control of smart composite plates using optimized self-tuning fuzzy logic controller with optimization of placement, sizing and orientation of PFRC actuators

Nemanja D. Zorić*, Aleksandar M. Tomović, Aleksandar M. Obradović, Radoslav D. Radulović, Goran R. Petrović

University of Belgrade, Faculty of Mechanical Engineering
Kraljice Marije 16, Belgrade, Serbia
**Corresponding author. Tel. +38162 295 677*
E-mail addresses: nzoric@mas.bg.ac.rs (N. Zorić), atomovic@mas.bg.ac.rs (A. Tomović), aobradovic@mas.bg.ac.rs (A. Obradović), rradulovic@mas.bg.ac.rs (R. Radulović), gpetrovic@mas.bg.ac.rs (G. Petrović)

Abstract. This paper deals with optimization of the sizing, location and orientation of the piezo-fiber reinforced composite (PFRC) actuators and active vibration control of the smart composite plates using particle-swarm optimized self-tuning fuzzy logic controller. The optimization criteria for optimal sizing, location and orientation of the PFRC actuators is based on the Gramian controllability matrix and the optimization process is performed by involving the limitation of the plates masses increase. Optimal configurations of five PFRC actuators for active vibration control of the first six modes of cantilever symmetric $((90°/0°/90°/0°)_S)$, antisymmetric cross-ply ((90°/0°/90°/0°/90°/0°/90°/0°)) and antisymmetric angle-ply ((45°/-45°/45°/-45°/45°/-45°/45°/-45°)) composite plates are found using the particle swarm optimization. The detailed analysis of influences of the PFRC layer orientation and position (top or bottom side of composite plates), as well as bending-extension coupling of antisymmetric laminates on controllabilities is also performed. The experimental study is performed in order to validate this behavior on controllabilities of antisymmetric laminates. The particle swarm-optimized self-tuning fuzzy logic controller (FLC) adapted for the multiple-input multiple-output (MIMO) control is implemented for active vibration suppression of the plates. The membership functions as well as output matrices are optimized using the particle swarm optimization. The Mamdani and the zero-order Takagi–Sugeno–Kang fuzzy inference methods are employed and their performances are examined and compared. In order to represent the efficiency of the proposed controller, results obtained using the proposed particle swarm optimized self-tuning FLC are compared with the corresponding results in the case of the linear quadratic regulator (LQR) optimal control strategy.

Keywords: Active vibration control, Smart composite plate, PFRC actuator optimization, Particle swarm optimization, Fuzzy logic control.

1. Introduction

Thin-walled composite structures have been extensively applied in various engineering fields like aeronautics, astronautics, automotive and military industry, robotics, sport equipment, medical engineering etc. due to their strength-to-weight and stiffness-to weight ratios. During exploitation, these structures are affected by various external disturbances causing the occurrence of undesirable vibrations, which can decrease performances and lead to damages. In the past decades, piezoelectric materials have been integrated in these structures as actuators and sensors, making together the so-called “smart structures”. This type of structures has the ability of adaptation to environmental conditions according to

the design requirements by detecting and responding to disturbances, which also includes detecting and reduction of undesirable vibrations (active vibration control). In order to increase actuating and sensing performances, piezoelectric fibers are usually stacked into a single layer composite, making the so-called piezo-fiber reinforced composite (PFRC) actuator and sensor, which provides high flexibility, durability and reliability [1]. Besides actuators and sensors, the applied control algorithm has a great impact on performances of smart structures. According to the previous statements, the design process of smart structures involves structural design of a base structure, proper sizing and placement of the actuators and sensors and controller design [2].

A large number of spacecraft structures can be modeled as a cantilever plate, like aircraft wings and empennages, helicopter and wind-turbine rotor blades, solar panels of spacecraft structures, flexible robotic manipulator, etc. Optimization of piezoelectric actuators for active vibration control of a plate has been studied by many researchers. The review of optimization criteria for optimal placement of piezoelectric sensors and actuators on smart structures is given in [3]. Kumar and Narayanan [4] presented the location optimization of piezoelectric actuators on steel plates by minimizing the linear quadratic regulator cost. Optimal locations were found by using the genetic algorithm (GA). Similar investigation was performed by Darivandi et al. [5], who applied the subgradient-based integer minimax optimization. Mentioned authors show that this optimization method is more accurate and considerably faster than the GA. Optimization criterion based on the controllability Gramian and GA for finding optimal locations of piezoelectric actuators was performed by Peng et al. [6] for aluminum plates and Han and Lee [7] for composite plates. Also, Han and Lee [7] considered minimizing controllability of residual modes in order to spillover prevention. Liu et al. [8] investigated optimal placement of piezoelectric actuators for active vibration control of a membrane structure by using the controllability Gramian and the particle swarm optimization (PSO) algorithm. They demonstrated that the computational efficiency of PSO is higher than that of GA. Halim and Moheimani [9] developed methodology for optimal placement of a collocated piezoelectric actuator–sensor pair on a plate by using modal and spatial controllability measures based on H_2 norm. Nestorović and Trajkov [10] presented a general approach for optimal actuator and sensor placement on steel plates based on the method for balanced model reduction, which results in models with equally controllable and observable controlled modes. The optimization criteria are based on the H_2 and the $H\infty$ norms which are calculated for all possible actuators and sensors locations. Chhabra et al. [11] used the modified control matrix and the singular value decomposition approach for optimal placement of ten piezoelectric actuators for active vibration control of the first six modes of steel plates. Optimal positions of the actuators are obtained by GA maximizing the fitness function based on the singular value of column control matrix. Quoc et al. [12] reported finding the optimal locations of the five monolithic piezoelectric actuator/sensor pairs to maximize the fundamental frequencies of composite plates using the GA. Also, effects of the orientations of plate layers, as well as plate geometry and boundary conditions on optimization results are analyzed. Daraji et al. [13] propose methodology for determination of the global optimal distribution of piezoelectric sensor/actuator pairs on steel plates based on maximum output voltage, when the structure is driven into the resonant modes. Correia et al. [14] implemented simulated annealing for optimal placement of eight piezoelectric actuators on composite plates in order to maximize the actuator performance by maximum plate deflection. Also, orientation of the plate layers is considered in optimization. Song et al. [15] analyzed influences of the placements of piezoelectric actuators and sensors on the active flutter control of composite laminated panels. All above mentioned papers [4-15] deal with the optimal placement of rectangular monolithic piezoelectric actuators with constant dimensions. Optimization problem is based on finding only the actuator location on a plate. Also, plates are divided into finite elements that have the same dimensions as the actuator. This allows the discrete optimal actuator location problem to be formulated as zero-one optimization problem. Orientation optimization of one monolithic piezoelectric actuator with constant dimensions on aluminum plate by using the Gramian controllability matrix and the fuzzy optimization strategy is presented in [16]. The actuator is placed at the root of the cantilever aluminum plate and optimal orientation is found for active vibration control of the first two modes. In paper [17], optimization of the piezoelectric actuator shape on composite plate is performed by minimizing the response of the system. Optimization problems

are solved with the use of evolutionary algorithms. The controllability index for optimal placement and sizing of piezoelectric patches on smart beams is given in [18]. Quek et al. [19] studied the problem of determining the optimal position and dimensions of piezoelectric actuator/sensor pairs on composite plates using two optimization performance indices based on modal and system controllability. The classical direct pattern search method is employed to obtain the optimal solutions. Bruant et al. [20] presented location and orientation optimization of piezoelectric actuators and sensors on steel plates by maximizing eigenvalues of the Gramian controllability and observability matrices of controlled modes and minimizing eigenvalues of the Gramian controllability and observability matrices for residual modes. Two optimization variables are considered for each piezoelectric device: the location of its center and its orientation. The optimization problem is solved by using the GA. The same optimization problem is solved by using the hybrid optimization approach based on the GA, the sequential quadratic programming (SQP) and the PSO combined with projected gradient techniques [21]. It is found that the solutions obtained by presented algorithm are better and with a better precision than those of Bruant et al. [20]. Qiu et al. [22] analyzed the effect of position and orientation of the piezoelectric actuators on controllability of bending and torsional modes of the cantilever aluminum plate. Controllability is measured by using H_2 norm. It is found that for suppressing bending modal vibration, the piezoelectric actuators should be located at the root of the plate, with orientation angle of 0^o and for suppressing torsional vibration, the sensors and actuators should be located at the tip of the plate, with orientation angle of 45^o. Ambrosio et al. [23] proposed maximizing H_2 norms of the controlled modes and minimizing H_2 norms of the residual modes for optimal placement and orientation of five piezoelectric actuators on composite plate clamped on three of its four sides. The GA is used to solve optimization problem. The same approach is described in [24] for active vibration control of simply supported aluminum plate in the cases where the first two modes are considered as controlled modes and the other three modes are considered as residual modes, and where the first three modes are considered as controlled modes and the other two modes are considered as residual modes. In [25] the authors used the performance index based on the Hankel singular values of the system and the PSO for optimization of the location and dimensions of piezoelectric actuators. Comparing PSO with GA, it was found that computation time of GA is about six times longer for 200 iterations and that GA cannot reach a good optimum point in a few iterations like the PSO. Optimization of positions and orientations of monolithic piezoelectric actuators for static shape control of beams and plates are shown in [26 - 29]. All above mentioned works [4-29] deal with the monolithic piezoelectric actuators. Due to their orthotropic properties, PFRC piezoelectric actuators show superior behavior over monolithic actuators for active vibration control. This superior behavior is presented by Azzouz et al. [30], where the influence of position and orientation of the monolithic and the PFRC piezoelectric actuator on actuation properties of the cantilever aluminum plate is investigated. It is shown that actuation of both bending and twisting amplitudes performed by PFRC is better compared to the monolithic actuator. Kapuria and Yasin performed active vibration suppression of hybrid fiber metal laminate (FML) rectangular [31] and skew [32] plates with integrated PFRC actuators and sensors. Top and bottom sides of the plates are fully covered with PFRC actuator and sensor layers, and they are electroded in segments and optimal orientation of each segmented part is found by plotting control voltages under step and impulse excitation. Paper [33] analyzes the active control of thermal buckling and vibration of a sandwich composite laminated plate with PFRC actuator. It is found that the critical buckling temperature of the structure can be maximized by optimizing the PFRC actuator fiber orientation. Also, the stability of the laminated composite plates can be significantly improved by combination of the active thermal buckling control and the vibration control strategy. Gohari et al. [34] investigated actuating properties of d_{31} and d_{33} PFRC actuators for shape control of simply supported and cantilever composite plates. Wang et al. [35] reported optimization of placement and orientation of the rectangular PFRC with fixed dimensions for active vibration control of a cantilever aluminum plate for three cases: bending control, twisting control, and coupled bending–twisting control. They also analyzed actuation effects of the actuators in the unimorph and the antisymmetric angle-ply bimorph configurations. The Gramian controllability matrix is applied as optimization criterion and optimal configurations are found by using the GA.

Apart from locations, sizes and orientations of piezoelectric actuators, the dynamic performance and functionality of smart structures depend on the applied control algorithm. Reviewing the available works related to active vibration control of flexible structures, it can be concluded that various control strategies are employed. The "Classical" control algorithms such as the constant gain velocity feedback or the constant gain position feedback are the most commonly employed. These algorithms for active vibration control of plates are applied in [4, 7, 12, 15, 19, 22-24, 31, 36-41]. The Proportional-Integer-Derivative (PID) control algorithm for active vibration control of smart flexible structures is investigated in [16, 42-44]. Combination of the fractional calculus and the classical control algorithm results in the fractional order (FO) control. Birs et al. [45] compared the integer order proportional-derivative (PD) and the FO PD control of flexible beam. Experimental results show that the FO PD controller is more robust than the integer one. The FO PD for active vibration control is also presented in [46, 47]. The FO positive position feedback compensator is studied in [48]. The optimal control algorithm such as the linear quadratic regulator (LQR) and the linear quadratic Gaussian (LQG) algorithms are also widely used for active vibration control of smart flexible plates [4, 5, 8, 10, 11, 13, 20, 32, 37, 44, 49-54]. The major disadvantage of the LQR and the LQG algorithms is the fact that they require an exact mathematical model of the structure. On the other side, the mathematical model used for controller design will not closely match the real system. The reason is ignorance of the exact parameters of materials, involving a number of assumptions in mathematical modeling, unmodeled dynamics or external disturbances, which results in that the designed controller may not achieve the desired performances and in some cases it can be unstable. In order to overcome this problem, some authors investigated active vibration control of flexible beams and plates using robust control techniques such as the H_2 [55], the H_∞ [56-59] and the sliding mode control [60]. Another alternative to cope with this problem is using the fuzzy set theory in controller design, which results in an intelligent robust controller with the ability to represent almost any deterministic controller. Nasser et al. [61] and Sharma et al. [62] investigated active vibration suppression of composite structures using a fuzzy logic controller (FLC). The FLC gives more flexibility to the designer and its main advantage is inherent robustness and ability to deal with uncertainties, imprecision and nonlinearities. On the other side, the precision of conventional FLC is not good and its adaptive ability is limited, which is especially manifested in a field of active vibration control of structures because external excitations make the vibrations have a stochastic nature. Wei et al. [63] demonstrated that a conventional FLC can suppress quickly large-amplitude to low-amplitude vibrations. Suppression of lower-amplitude vibrations can be achieved by change of the membership function destiny, but low-amplitude residual vibration cannot be damped out completely. In order to avoid this disadvantage, authors combined fuzzy and PI controller making a dual mode controller. Si and Li [64] overcame disadvantages and improved the conventional FLC performances using scaling universes of discourse method. Zorić et al. [65, 66] presented the optimized self-tuning FLC of smart composite beams. In the proposed FLC, the scaling factors of input variables (modal displacement and modal velocity) are adjusted via peak observer. The membership functions are parameterized and optimal configuration of these parameters is found using the PSO algorithm. Similar approach for self-tuning FLC is applied for vibration control of the magnetorheological elastomer vibration isolation system [67].

Reviewing available articles related to the optimization of piezoelectric actuators, it can be concluded that, to the best of our knowledge, no study has been reported on the simultaneous optimization of sizing, location and orientation of the PFRC actuators on composite plates. The first part of this paper deals with simultaneous optimization of the sizing, location and orientation of the PFRC actuators on symmetric, antisymmetric cross-ply and antisymmetric angle-ply composite plates. The objective function is based on the Gramian controllability matrix and the optimization process is performed by involving the limitation of the plates masses increase. Optimal configurations are found by using the PSO algorithm. The detailed analysis of influences of the PFRC layer orientation and position (top or bottom side of composite plates), as well as bending-extension coupling of antisymmetric laminates on controllabilities is also performed. The experimental study is performed in order to validate this behavior on controllabilities of antisymmetric laminates. In the second part of the paper the active vibration control of smart composite plates using the PSO optimized self-tuning FLC is presented.

Adaptation of the control algorithm, presented by Zorić et al. [65], for active vibration suppression of composite plates in the multiple-input multiple-output (MIMO) manner is performed. Also, members of the output matrices are optimized using PSO algorithm. The Mamdani and zero-order Takagi–Sugeno–Kang fuzzy inference methods are employed and their performances are examined and compared. The results obtained using the proposed PSO optimized self-tuning FLC are compared with the corresponding results in the case of the LQR optimal control strategy.

2. Mathematical modeling and finite element discretization

Figure 1 presents the composite plate composed of a finite number of layers of uniform thickness with symmetrically distributed PFRC patches on the top and bottom side. Both elastic and piezoelectric layers are supposed to be thin, such that a plane stress state can be assumed. After discretization by using the finite element method based on the third-order shear deformation theory and modal analysis [68, 69], the following equation in modal coordinates is obtained:

$$\{\ddot{\eta}\}+[\Lambda]\{\dot{\eta}\}+\left[\omega^2\right]\{\eta\}=[\Psi]^{\mathrm{T}}\{F_{\mathrm{m}}\}-[\Psi]^{\mathrm{T}}\left[K_{\mathrm{me}}\right]_{\mathrm{A}}\{\varphi\}_{\mathrm{AA}}\,, \tag{1}$$

where $\{\eta\}$ represents the vector of modal coordinates, $\left[\omega^2\right]$ is the diagonal matrix of the squares of the natural frequencies, $[\Psi]$ is the modal matrix, and

$$[\Lambda]=\underset{i=1,r}{\mathrm{diag}}\left(2\zeta_i\omega_i\right) \tag{2}$$

is the modal damping matrix, where ζ_i is natural modal damping ratio of the i-th mode. Eq. (1) can be expressed in a state-space form in the following way

$$\left\{\dot{X}\right\}=[A]\{X\}+[B]\{\varphi\}_{\mathrm{AA}}+\{d\}\,, \tag{3}$$

where

$$\{X\}=\begin{Bmatrix}\eta\\ \dot{\eta}\end{Bmatrix},\ [A]=\begin{bmatrix}[0] & [\mathrm{I}]\\ -\left[\omega^2\right] & -[\Lambda]\end{bmatrix},\ [B]=\begin{bmatrix}[0]\\ \left[\bar{B}\right]\end{bmatrix}=\begin{bmatrix}[0]\\ -[\Psi]^{\mathrm{T}}\left[K_{\mathrm{me}}\right]_{\mathrm{A}}\end{bmatrix},\ \{d\}=\begin{bmatrix}[0]\\ [\Psi]^{\mathrm{T}}\{F_{\mathrm{m}}\}\end{bmatrix} \tag{4}$$

is the state vector, the system matrix, the control matrix and disturbance vector, respectively, where $[\mathrm{I}]$ and $[0]$ are the appropriately dimensioned identity and zero matrix, respectively.

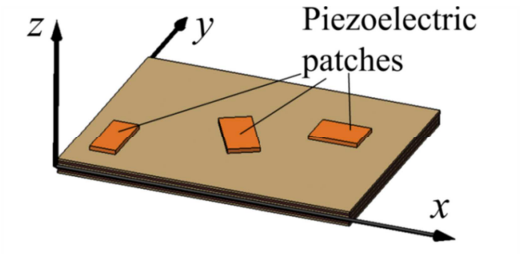

Fig. 1. Composite plate with PFRC patches.

2.1 Vibrational modes of cantilever composite plates

In this subsection, the quadratic cantilevers symmetric and antisymmetric cross and angle-ply laminated plates are considered. Dimensions of the plates are 0.5m x 0.5m and they consist of eight graphite-epoxy layers with the following orientations:

- symmetric composite plate: $(90°/0°/90°/0°)_S$,
- antisymmetric cross-ply composite plate: (90°/0°/90°/0°/90°/0°/90°/0°),
- antisymmetric angle-ply composite plate: (45°/-45°/45°/-45°/45°/-45°/45°/-45°).

The thickness of each layer is 0.25mm. Material properties of the graphite-epoxy layer are presented in Table 1. Natural frequencies of the first six modes of plates are given in Table 2. Modal shapes of the first six vibrational modes are illustrated in Figure 2 for symmetric composite plate, in Figure 3 for antisymmetric cross-ply composite plate, and in Figure 4 for antisymmetric angle-ply composite plate. For this purpose, the plates are discretized into 50x50 finite elements.

Table 1
Material properties of graphite-epoxy.

$E_1\,(\mathrm{GPa})$	174
$E_2\,(\mathrm{GPa})$	10.3
$G_{13}\,(\mathrm{GPa})$	7.17
$G_{23}\,(\mathrm{GPa})$	6.21
ν_{12}	0.25
$\rho\left(\mathrm{kgm}^{-3}\right)$	1389.23

Table 2
Natural frequencies of the first six modes of plates.

Symmetric plate						
Mode	1	2	3	4	5	6
Frequency (Hz)	8.628	14.54	54.069	62.908	81.181	114.663
Antisymmetric cross-ply plate						
Mode	1	2	3	4	5	6
Frequency (Hz)	10.369	15.747	64.949	70.531	72.474	113.226
Antisymmetric angle-ply plate						
Mode	1	2	3	4	5	6
Frequency (Hz)	7.012	25.814	41.186	69.696	84.667	125.914

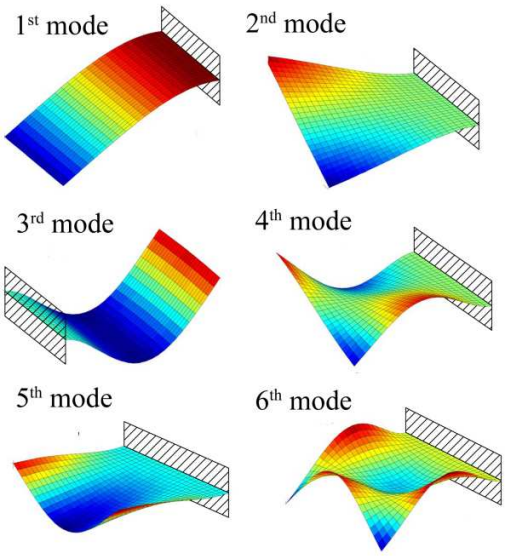

Fig. 2. Modal shapes of the first six vibrational modes for symmetric composite plate.

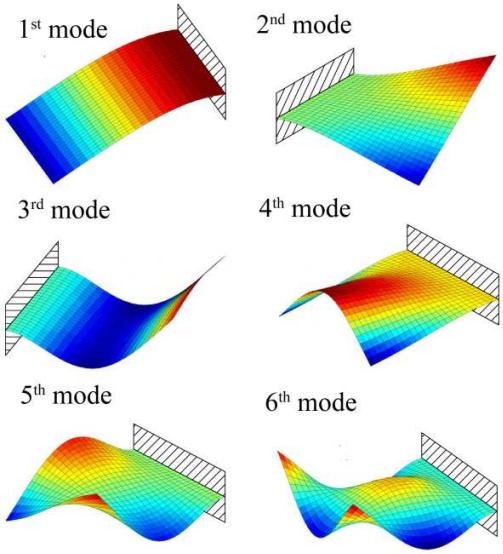

Fig. 3. Modal shapes of the first six vibrational modes for antisymmetric cross-ply composite plate.

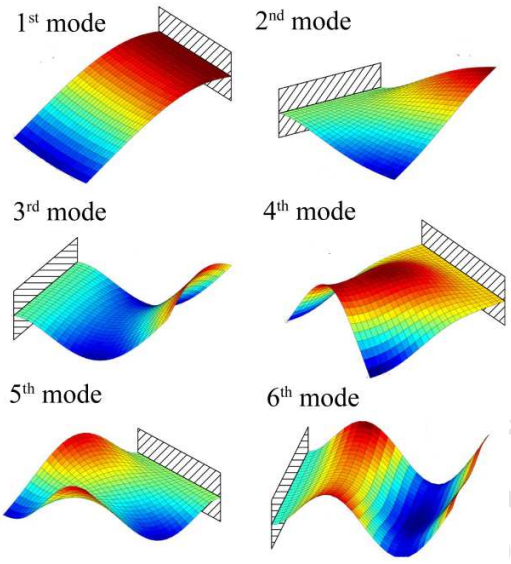

Fig. 4. Modal shapes of the first six vibrational modes for antisymmetric cross-ply composite plate.

3. Influence of PZT actuator orientation on controllability

Controllability is a structural property and it can be defined as a system ability to control all states of given system. It depends of system dynamics and the location, size, orientation and number of actuators. For active vibration control, the controllability of the entire system is a combination of controllability of individual modes and it can be expressed quantitatively by using the Gramian controllability matrix. When structural damping is small, the controllability Gramian expressed in modal coordinates is diagonally dominant [70].

$$[W_{\mathrm{C}}]=\begin{bmatrix} W_{\mathrm{C}11} & 0 & \cdots & 0 \\ 0 & W_{\mathrm{C}22} & \cdots & 0 \\ \vdots & \vdots & \ddots & \vdots \\ 0 & 0 & \cdots & W_{\mathrm{C}nn} \end{bmatrix}= \begin{bmatrix} \dfrac{1}{4\zeta_1\omega_1}\left(\overline{B}\right)_1\left(\overline{B}\right)_1^{\mathrm{T}} & 0 & \cdots & 0 \\ 0 & \dfrac{1}{4\zeta_2\omega_2}\left(\overline{B}\right)_2\left(\overline{B}\right)_2^{\mathrm{T}} & \cdots & 0 \\ \vdots & \vdots & \ddots & \vdots \\ 0 & 0 & \cdots & \dfrac{1}{4\zeta_n\omega_n}\left(\overline{B}\right)_n\left(\overline{B}\right)_n^{\mathrm{T}} \end{bmatrix}, \tag{5}$$

where $\left(\overline{B}\right)_i$ is the *i*-th row of matrix $\left[\overline{B}\right]$. The value of this diagonal term gives information about the energy transmitted from the actuators to the structure for active control of the corresponding mode. In order to control several modes simultaneously, Hac and Liu [70] presented the performance index:

$$J_{\mathrm{e}} = \mathrm{trace}\left([W_{\mathrm{C}}]\right)\left(\det\left([W_{\mathrm{C}}]\right)\right)^{1/(2Nc)}, \tag{6}$$

where N_{C} is the number of controlled modes.

Controllability of composite plates, apart from dimensions of piezoelectric actuators, depends on its orientation, especially when the PFRC actuator is used. Due to this fact, the next aim is to examine the influence of the actuator layer orientation on controllability. For this purpose, the PFRC layers are symmetrically placed and cover the entire top and bottom side of the plate and its orientation (Θ_{A}) varies from -90º to 90º. Piezoelectric fibers of the PFRC actuator are made of PZT5A, and the actuator properties are given in Table 3.

Table 3
Material properties of PFRC layer.

$E_1\left(\mathrm{GPa}\right)$	30.2
$E_2\left(\mathrm{GPa}\right)$	14.9
$G_{13}\left(\mathrm{GPa}\right)$	5.13
$G_{23}\left(\mathrm{GPa}\right)$	5.13
ν_{12}	0.45
$\rho\left(\mathrm{kgm}^{-3}\right)$	4600
$e_{31}\left(\mathrm{Cm}^{-2}\right)$	9.41
$e_{32}\left(\mathrm{Cm}^{-2}\right)$	0.166
$k_{33}\left(\mathrm{Fm}^{-1}\right)$	$6.1\mathrm{x}10^{-9}$

3.1 Symmetric composite plate

Figures 5 and 6 show diagonal terms of the Gramian controllability matrix for the first six modes and the performance index versus orientation angle of the actuator layer, respectively. From these figures it is noticeable that the diagonal terms of the Gramian controllability matrix and the performance index are equal for opposite orientation angles ($+\Theta_{\mathrm{A}}$ and $-\Theta_{\mathrm{A}}$), due to symmetry. Also, comparing Figure 5 and Figure 2, it can be concluded that maximal controllability for a particular mode is achieved when the PFRC actuator fibers are oriented in the direction of the plate deformation for this mode (0° for the 1st and the 3rd, 90° for the 5th and 6th, ±45° for the 2nd and ±35° for the 4th mode). Also, the controllability does not exist when the modal line presents symmetry of the piezoelectric actuator [71] (0° and 90° for the 2nd and the 4th, 90° for the 1st and the 3rd and 0° for the 5th and the 6th mode). Due to that, the performance index is zero for orientations of 0° and 90°, and reaches the maximum value for orientation ±40° (Fig. 6).

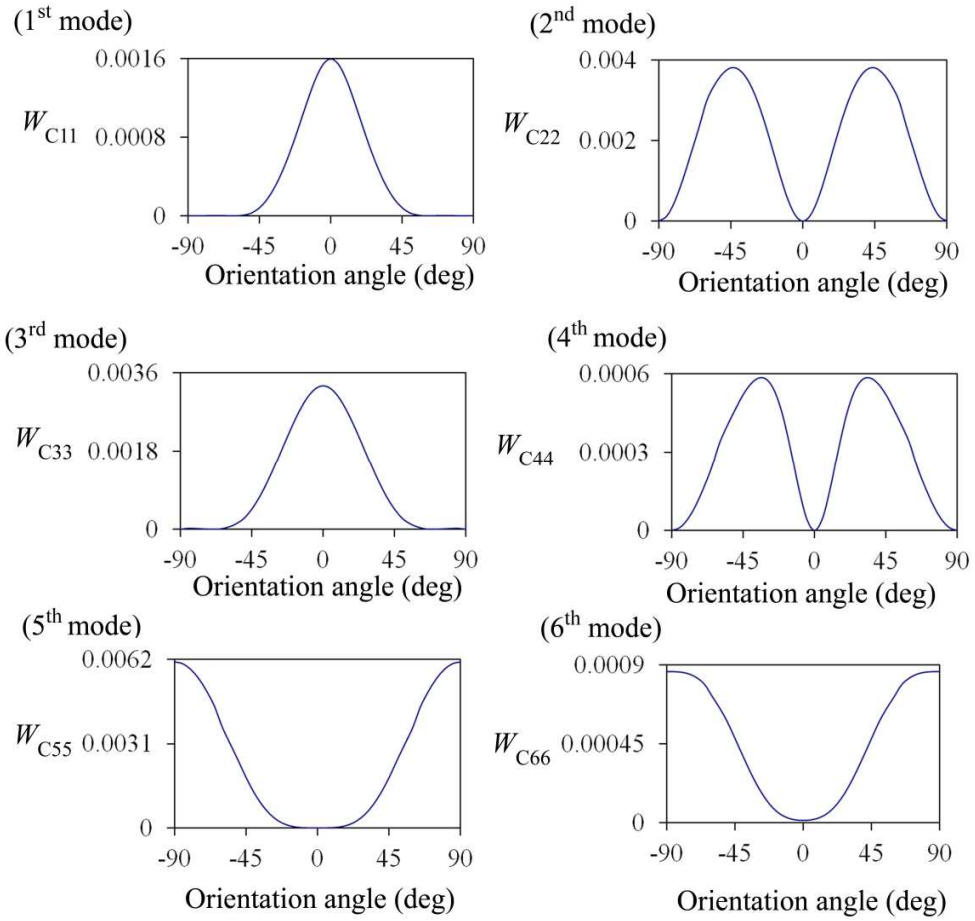

Fig. 5. Diagonal terms of the Gramian controllability matrix for the first six modes versus orientation angle of the actuator layer for the symmetric composite plate.

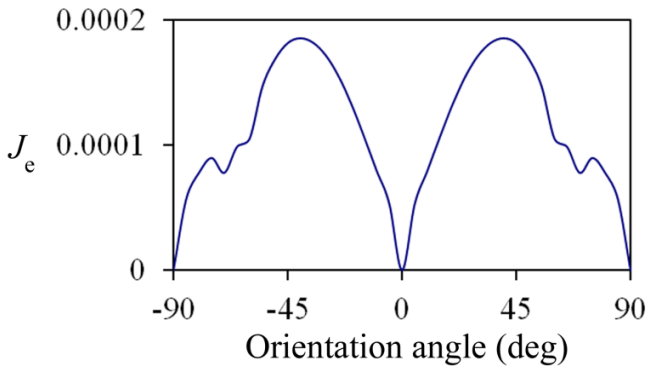

Fig. 6. Performance index versus orientation angle of the actuator layer for the symmetric composite plate.

3.2 Antisymmetric cross-ply composite plate

Figures 7 and 8 display diagonal terms of the Gramian controllability matrix for the first six modes and the performance index versus orientation angle of the actuator layer, respectively. According to the Figures 7 and 3, it can be concluded as in the previous case: maximum controllability is achieved when the PFRC actuator fibers are oriented in the direction of the plate deformation for this mode. In this case, it is also noticeable that the diagonal terms of the Gramian controllability matrix and the performance index are equal for opposite orientation angles ($+\Theta_A$ and $-\Theta_A$), but unlike for the previous case, there is a significant difference, depending on whether the actuator is placed on the top or the bottom side of the plate. The reason for that is the bending-extension behavior of antisymmetric cross-ply composites (bending-extension coupling stiffnesses B_{11} and B_{22} are not zero [72]), which leads to the larger strain on one side of the plate than on the opposite side, resulting in non-symmetry of the controllability. Also, by symmetrical integration of PFRC layers, shear-extension (A_{16} and A_{26}) as well as bending-twisting (D_{16} and D_{26}) coupling stiffnesses are not zero for $\Theta_A \neq 0^\circ$ and $\Theta_A \neq 90^\circ$, which also contributes to non-symmetry of the controllability. For the 1st and the 3rd mode, the controllability is higher if the actuator is placed at the bottom side (maximum value is reached for the orientation of 0°). This is a contribution of B_{11} bending-extension coupling stiffness. For the 4th, 5th and 6nd mode, the controllability is higher if the actuator is placed on the top side because B_{22} bending-extension coupling stiffness, which causes this effect, is the opposite to B_{11} (B_{22}=- B_{11}). Maximum controllability is reached for the orientation of ±70° for 4th mode and 90° for the 5th and the 6th mode. For the 2nd mode, controllability is slightly higher if the actuator is placed at the bottom side due to a small value of bending-twisting coupling stiffnesses caused by PFRC layers. The maximum value is reached for the orientation of ±45°. From aforementioned, it can be concluded that there is higher controllability when the actuator is placed on the side, where the angle between the actuator fibers and the fibers of the layer in contact has a larger value.

The value of the performance index is 0 for angles 0° and 90° (Fig. 8). It is evident, because the diagonal term of the Gramian controllability matrix for some modes is 0 for these angles. The performance index is larger when the actuator is placed at the bottom side for the angles between -35° and 35° and a small interval around -60° and 60°. For other angles this index is larger when the actuator is placed on the top side. Its maximum value is reached for angles ±40° when the PFRC actuator is placed on the top of the plate.

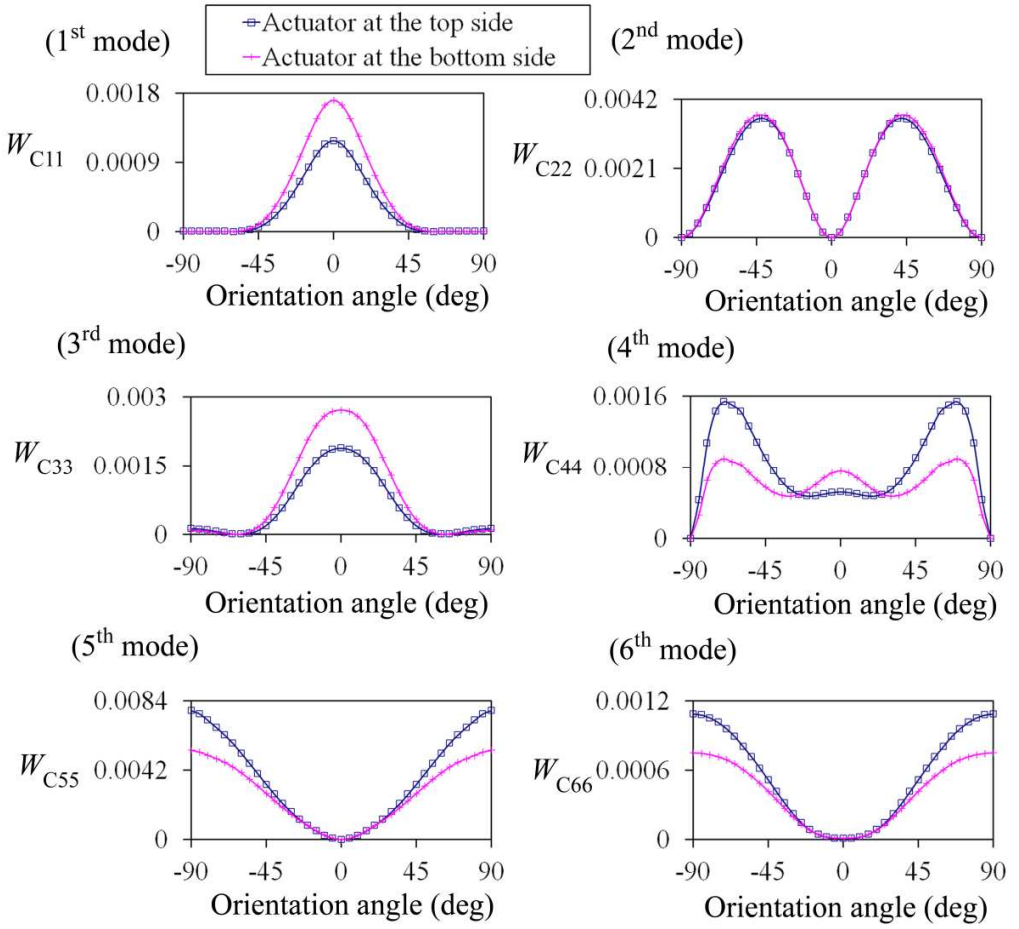

Fig. 7. Diagonal terms of the Gramian controllability matrix for the first six modes versus orientation angle of the actuator layer for the antisymmetric cross-ply composite plate.

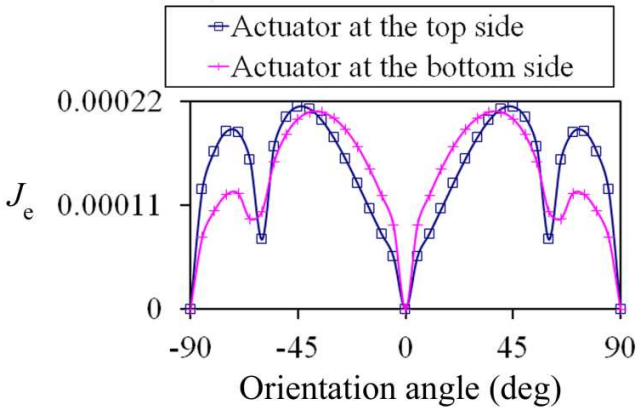

Fig. 8. Performance index versus orientation angle of the actuator layer for the antisymmetric cross-ply composite plate.

3.3 Antisymmetric angle-ply composite plate

The following analysis is performed for the cantilever antisymmetric angle-ply composite plate. Figure 9 presents diagonal terms of the Gramian controllability matrix of controlled modes versus orientation angle of the actuator layer, while Figure 10 presents the performance index versus orientation angle of the actuator layer. For this type of orientatnon the same conclusion can be drawn as for two previous cases, the maximal controllability is reached when the PFRC actuators fibers are oriented in the direction of deformation for a corresponding mode (comparing Figs. 9 and 4).

Unlike in the previous case, diagonal terms of the Gramian controllability matrix are not symmetric with respect to orientation angle, especially for the 2nd and the 5th mode. Better controllability is achieved when fibers orientation of the actuator layer is opposite the orientation of the layer in contact (in relation to the *x* axis). Again, the reason is bending-extension coupling (bending-extension coupling stiffnesses B_{16} and B_{26} are not zero [72]). Also, by symmetrical integration of PFRC layer, shear-extension (A_{16} and A_{26}), as well as bending-twisting (D_{16} and D_{26}) coupling stiffnesses are not zero for $\Theta_A \neq 0^\circ$ and $\Theta_A \neq 90^\circ$, which also contributes to non-symmetry of the controllability. It is noticeable that when the actuator is orientated at the angle of $+\Theta_A$, controllability at the top of the plate is equal to controllability when the actuator is set at the angle of $-\Theta_A$ at the bottom of the plate, and vice versa. Thus, maxium controllability for the 2nd mode is achieved if the actuator is placed at the bottom side with the orientaton of -45º (or on the top side with the orientation of 45º), and for the 5th mode if the actuator is placed at the bottom side with the orientaton of -55º (or on the top side with the orientation of 55º). For the 4th mode, controllability reaches maximum for the orientations of ±90º and minimum for the orientation of 0º. This minimum controllability for 0º is not 0, because of the coupling stiffnesses of PFRC layers. Also, due to coupling stiffnesses, maximum controllabilities for the 1st and the 6th mode are not for the orientation of 0º, but for ±5º (depending on the location of the actuator).

From Figure 10 it can be concluded that the performance index reaches the highest value for the angle of 25° in the case when the actuator is positioned on the top side and for the angle of -25° in the case when the PFRC actuator is placed at the bottom side of the plate.

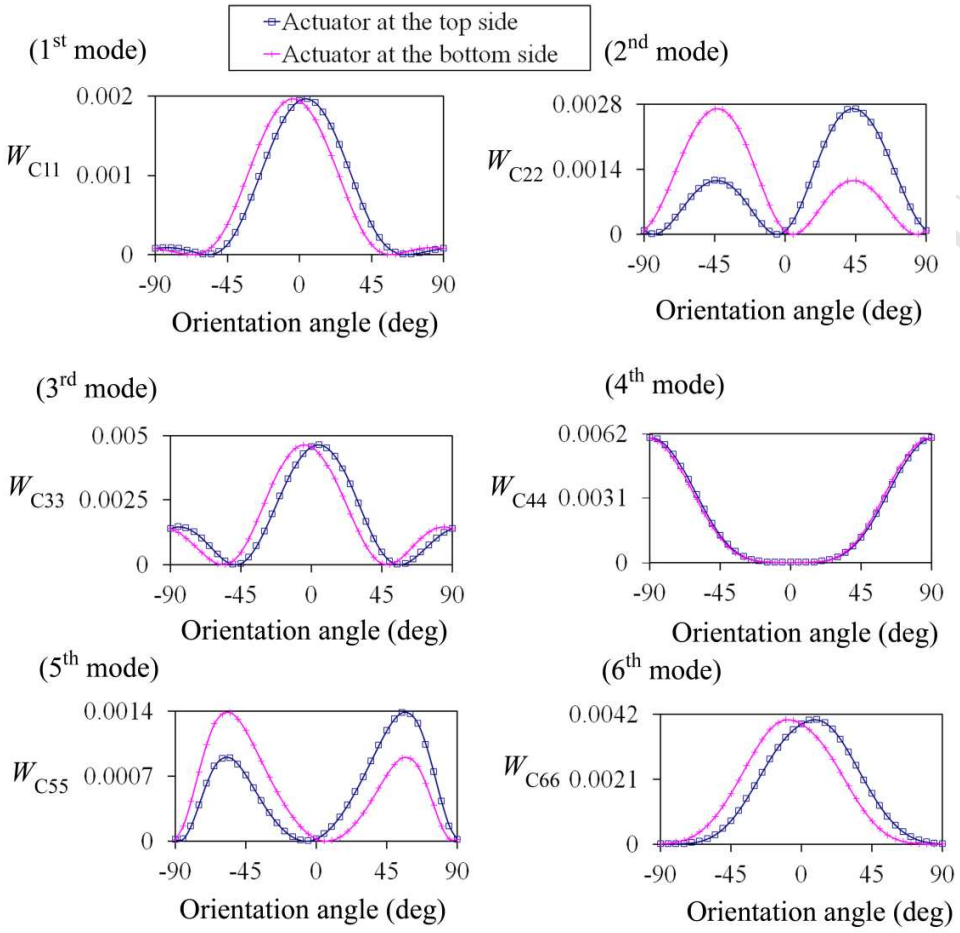

Fig. 9. Diagonal terms of the Gramian controllability matrix for the first six modes versus orientation angle of the actuator layer for the antisymmetric angle-ply composite plate.

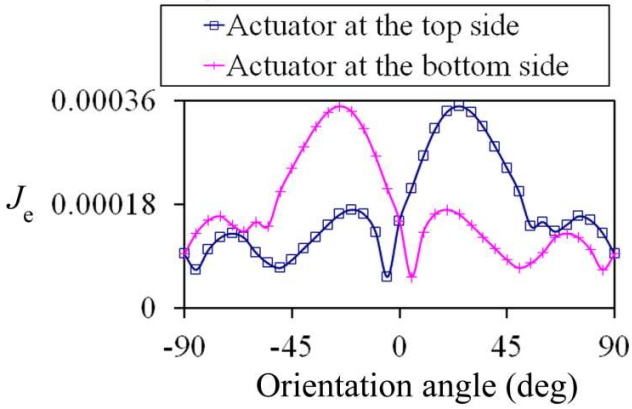

Fig. 10. Performance index versus orientation angle of the actuator layer for the antisymmetric angle-ply composite plate.

4. Optimization of the sizing and orientation of PFRC actuators

One of the goals of this paper is to find the positions, sizes and orientation of selected number of PFRC actuators for achieving maximum controllability. Since integration of these actuators leads to the increasing of the plate mass, appropriate constraints will be involved. Figure 11 presents the cantilever composite plate with the integrated *i*-th actuator, where a and b are dimensions of the plate, x_i and y_i present the actuator center position with respect to the coordinate system of the plate, a_i and b_i are dimensions of the actuator, and Θ_{Ai} is its orientation. The actuator and sensor patches are symmetricaly placed (each sensor has equal size, position and orientation as the corresponding actuator, but it is placed on the opposite side of the plate).

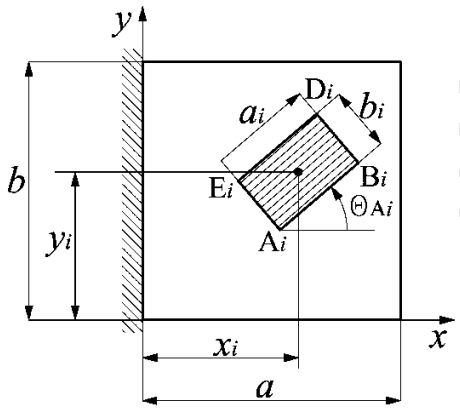

Fig. 11. Composite plate with the *i*-th PFRC actuator.

Constraints of the optimization problem can be defined as follows

- position constraints:

$$0 \le x_{Ai}, x_{Bi}, x_{Di}, x_{Ei} \le a, \quad 0 \le y_{Ai}, y_{Bi}, y_{Di}, y_{Ei} \le b, \qquad i = 1,\ldots,N_P , \tag{7}$$

  where N_P presents the number of piezoelectric actuators;

- constraints limiting the increase of the entire surface mass can be represented by the coverage of the plate surface:

$$\frac{\sum_{i=1}^{N_P} a_i b_i}{ab} \le \varepsilon \ , \tag{8}$$

  where ε presents the tolerance of the surface coverage;

- dynamic constraints which do not allow the overlapping of the actuators.

Taking into account the defined constraints, the objective function can be formulated as follows

$$OBJ = \text{maximize}\left(\overline{J}_{\text{e}}\right), \quad \overline{J}_{\text{e}} = \begin{cases} J_{\text{e}}, & \text{if constraints are not violated} \\ 0, & \text{if any constraint is violated} \end{cases}. \tag{9}$$

The presented optimization problem will be solved using the Particle swarm optimization method [73]. According to variables which define the size, position and orientation of each actuator, the *i*-th particle in the *k*-th iteration is defined by the following coordinates

$$\left[p_i^k \right] = \begin{bmatrix} x_{1i}^k & y_{1i}^k & a_{1i}^k & b_{1i}^k & \Theta_{\text{A}1i}^k \\ \vdots & \vdots & \vdots & \vdots & \vdots \\ x_{N_{\text{P}}i}^k & y_{N_{\text{P}}i}^k & a_{N_{\text{P}}i}^k & b_{N_{\text{P}}i}^k & \Theta_{\text{A}N_{\text{P}}i}^k \end{bmatrix}. \tag{10}$$

A particle changes its position and velocity in the following way

$$\begin{aligned} v_{id}^{k+1} &= \chi v_{id}^k + c_1 rand_{\,1}\left(lbest_{id} - p_{id}^k \right) + c_2 rand_{\,2}\left(gbest_d - p_{id}^k \right), \\ p_{id}^{k+1} &= p_{id}^k + v_{id}^{k+1}, \; i = 1, \ldots, n_{\text{POP}} \quad d = 1, \ldots, m \end{aligned} \tag{11}$$

where χ is inertia weight, c_1 and c_2 are the cognition and the social learning factors, respectively, $rand_{\,1}$ and $rand_{\,2}$ are random numbers between 0 and 1, n_{POP} is the number of the population, m is the population size, and $lbest$ and $gbest$ are the best local and global positions of the particle, respectively. For the actuator sizing and placement it is found that the best solution is obtained when the cognition and social learning factors are set to be 1.5 [2].

In forward numerical examples, the number of actuators is set to be 5, which leads to 25 parameters that have to be determined during optimization process. Analyzing the controllabilities for particular modes (Figs. 5, 7 and 9), it can be inferred that some modes have maximum controllability for the orientation of 0º, and some for the orientation of 90º. In order to reduce the number of optimization parameters, which will lead to the increase of computing effectiveness, the positions of three actuators are fixed: the first two actuators have equal dimensions, they are placed at the root of the plate and orientated with 0º; the third actuator is placed in the middle of free end of the plate and orientated with 90º (Fig. 12). The number of parameters is reduced from 25 to 14. Thus, coordinates of the *i*-th particle in the *k*-th iteration can be written as follows

$$\left[p_i^k \right] = \left[p_{1i}^k \quad p_{2i}^k \quad \cdots \quad p_{14i}^k \right], \tag{12}$$

In the case of the antisymmetric cross-ply plate, the first two actuators are placed at the bottom of the plate. The third actuator is at the top of the plate. If the orientation of the 4$^{\text{th}}$ and the 5$^{\text{th}}$ actuators is between -35º and 35º, they will be placed at the bottom side and in other cases at the top of the plate.

For the antisymmetric angle-ply plate, the first three actuators are placed at the top of the plate. The other two actuators will be placed at the top side for positive orientation and 0º, and at the bottom side for negative orientation.

The tolerance of the surface coverage is set to be 0.15 (15% of the surface is covered by PFRC patches).

Sizes, positions and orientations of the piezoelectric actuators are shown in Figure 13 and Table 4. Regarding the obtained angles of orientations of the 4$^{\text{th}}$ and 5$^{\text{th}}$ actuators for the antisymmetric cross-ply and the antisymmetric angle-ply plate, they are placed on the top side of these plates. Table 5 presents

diagonal values of the Gramian controllability matrix and performance index for the obtained solutions. Besides obtained configuration for the antisymmetric cross-ply plate cases (the first two actuators at the bottom side, and the other three on the top side), when all five actuators are placed on the top and at the bottom side of the plate, are also given (Table 5) in order to compare these results and show that obtained configuration leads to better controllability compared to the situation when all actuators are on one side of the plate.

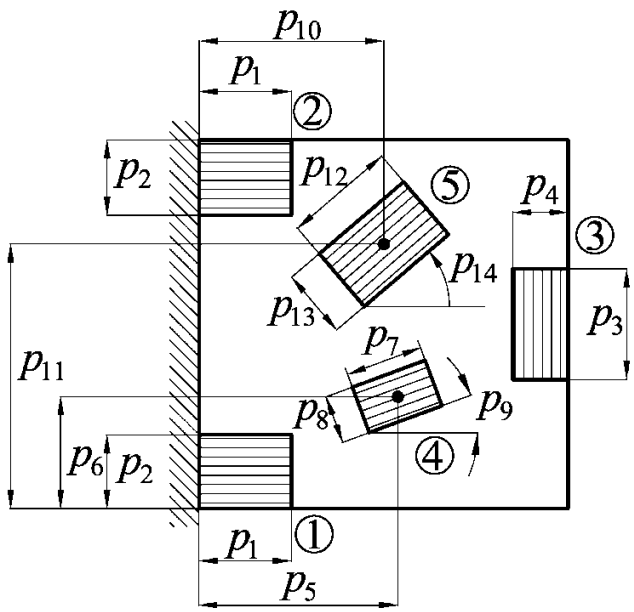

Fig. 12. Optimization parameters of PFRC actuators.

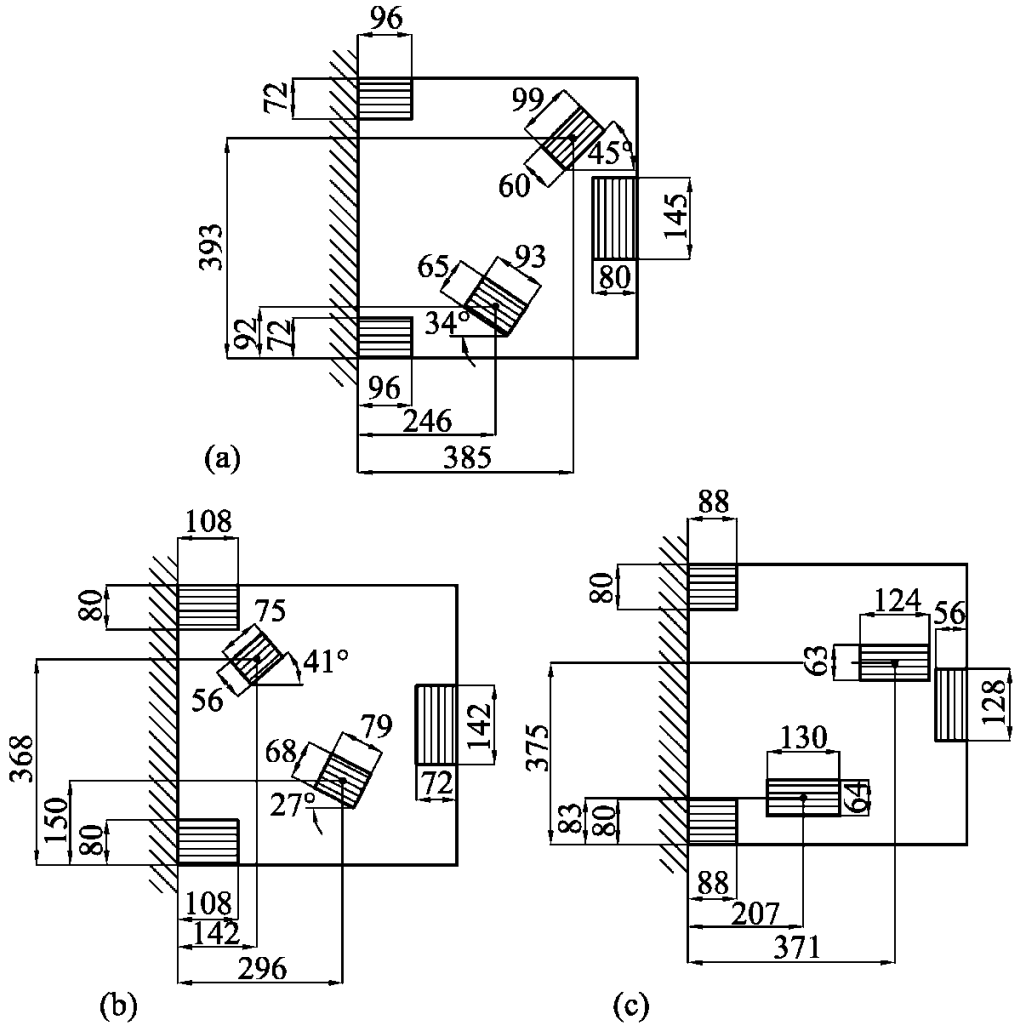

Fig. 13. Sizes, locations and orientations of the actuators obtained by optimization. (a) Symmetric plate; (b) Antisymmetric cross-ply plate; (c) Antisymmetric angle-ply plate.

Table 4
Sizes, positions and orientations of piezoelectric actuators.

	Symmetric plate	Antisymmetric cross-ply plate	Antisymmetric angle-ply plate
$p_1(mm)$	96	108	88
$p_2(mm)$	72	80	80
$p_3(mm)$	145	142	128
$p_4(mm)$	80	72	56
$p_5(mm)$	246	296	207
$p_6(mm)$	92	150	83
$p_7(mm)$	93	79	130
$p_8(mm)$	65	68	64
$p_9(^\circ)$	-34	-27	0
$p_{10}(mm)$	385	142	371
$p_{11}(mm)$	393	368	375
$p_{12}(mm)$	99	75	124
$p_{13}(mm)$	60	56	63
$p_{14}(^\circ)$	45	41	0

Table 5
Diagonal values of the Gramian controllability matrix and performance index obtained by the PSO optimization.

	Symmetric plate	Antisymmetric cross-ply plate			Antisymmetric angle-ply plate
		Obtained configuration	All actuators at the top side	All actuators at the bottom side	
$W_{C11}\left(\times 10^{-3}\right)$	0.0148	0.0242	0.0167	0.0242	0.0198
$W_{C22}\left(\times 10^{-3}\right)$	0.0392	0.0512	0.037	0.0512	0.0354
$W_{C33}\left(\times 10^{-3}\right)$	0.0517	0.0809	0.0586	0.0775	0.1443
$W_{C44}\left(\times 10^{-3}\right)$	0.1137	0.1929	0.1929	0.1368	0.079
$W_{C55}\left(\times 10^{-3}\right)$	0.1977	0.1196	0.0837	0.1194	0.134
$W_{C66}\left(\times 10^{-3}\right)$	0.1884	0.1736	0.1532	0.1414	0.2596
$J_e\left(\times 10^{-6}\right)$	5.1	5.954	4.424	4.861	6.041

5. Experimental study

For experimental validation of theoretical and numerical results obtained about controllabilities, the cantilever antisymmetric cross-ply composite plate, made of two 400g/m^2 unidirectional carbon layers with orientations (90°/0°) (from bottom to top) is considered. Dimensions of the plate are 200 mm x 200 mm. The number of actuators is one, whereas the first three natural modes are considered as controlled modes. The selected PFRC actuator is M8514-P2 made by "Smart Materials Corp."

The optimal position and orientation of the PFRC actuator is presented in Figure 14. Since obtained orientation is 0°, it is placed at the bottom side of the plate. In order to validate the influence of the bending-extension coupling on controllability, another actuator is placed on the top of the plate, symmetrically to the previous one (Figure 15).

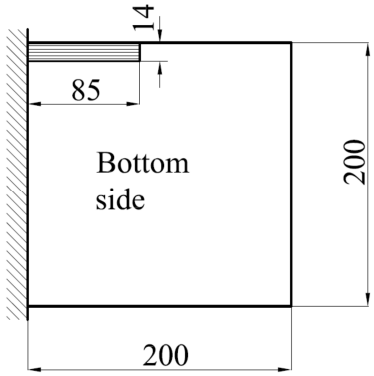

Fig. 14. Optimal position and orientation of the M8514-P2 PFRC actuator.

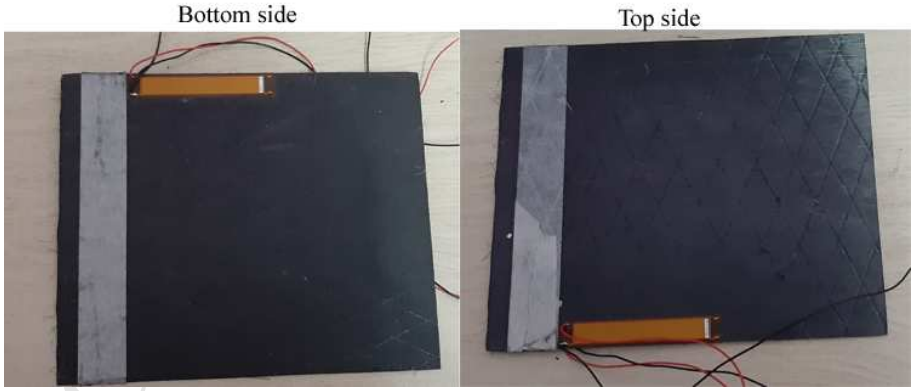

Fig. 15. The composite plate with integrated M8514-P2 PFRC actuators.

In order to compare controllabilities of the actuators, the sine test is performed. Each actuator is driven by sine signal generated by a signal generator around the 1st, 2nd and 3rd natural frequencies and the response is measured by acellelometer positioned at the corner of the free side of the plate (Figure 16). The actuator with better controllability of a particular mode will cause better ecxitation of this mode. Maximum allowable voltage for M8514-P2 PFRC actuator is -60V - +360V. In this case, the actuators will be symmetrically loaded, between -60V - +60V. The custom-made voltage amplifier is employed to amplify the voltage from a signal generator. The experimental setup is presented in Figure 17.

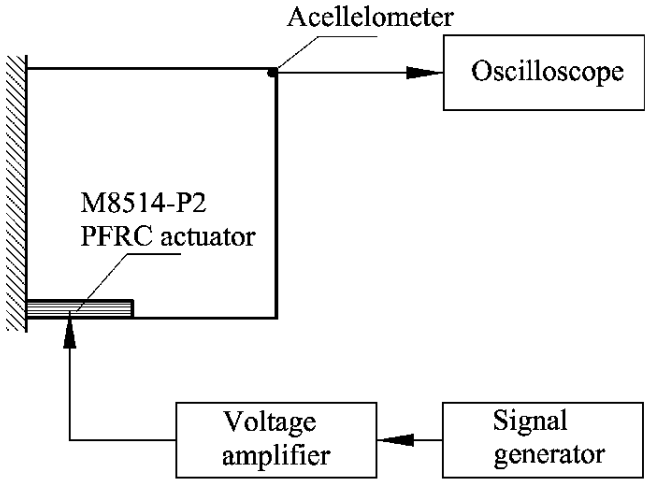

Fig. 16. Schematic diagram of the experimental setup.

Fig. 17. The experimental setup.

Figure 18 presents peak-to-peak voltages of the output signal obtained by excitation of each actuator for frequencies around the 1st, the 2nd and the 3rd modes.

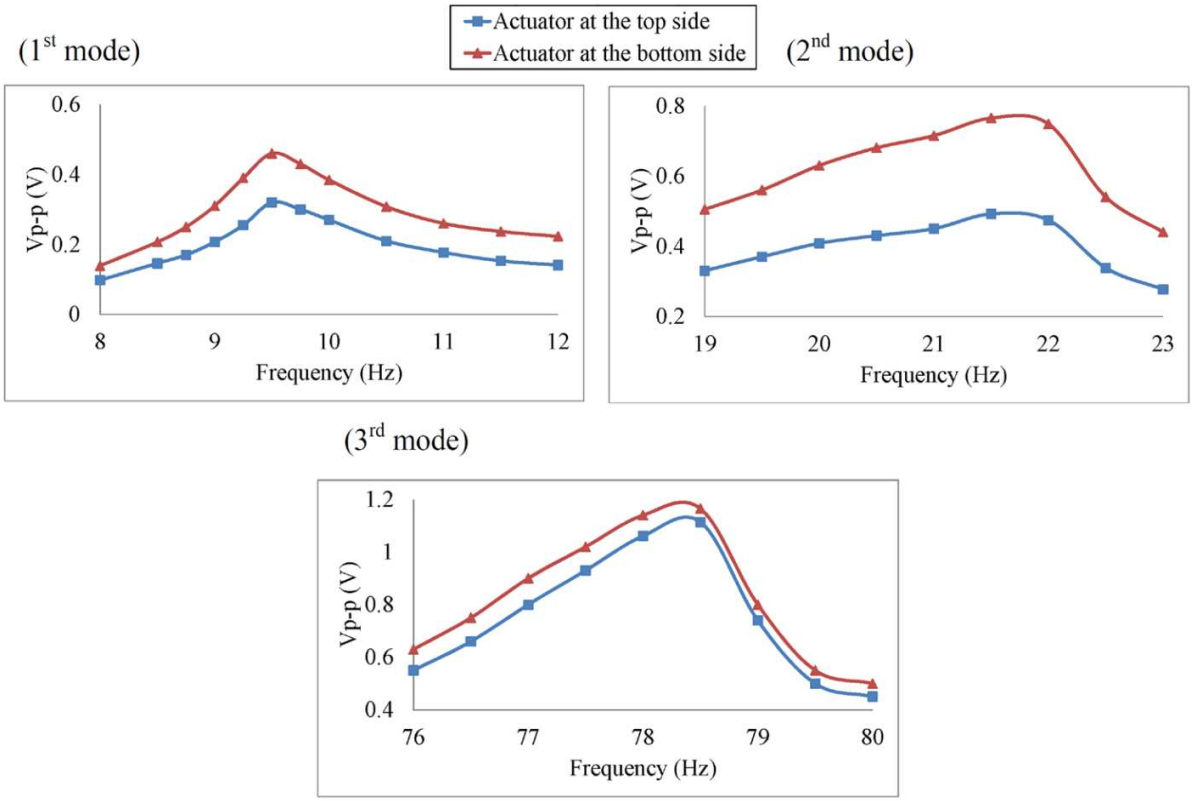

Fig. 18. Peak-to-peak voltages of the output signal for the 1st, the 2nd and the 3rd modes.

From Figure 18 it can be concluded that the actuator placed at the bottom of the plate provides better controllability for all three modes, which verifies the results obtained from numerical analysis.

6. Optimized self-tuning fuzzy logic control

Particle swarm optimized self-tuning logic controller is shown in [65], where the membership functions for both the Mamdani and the zero-order TSK inference method were parameterized and the parameters were found by using the Particle swarm optimization. Main idea of this control algorithm is tuning of the scaling factors of modal displacement (K_{d}) and modal velocity (K_{v}) during active vibration suppression through the self-tuning mechanism based on peak observer (modal displacement (η) and modal velocity ($\dot{\eta}$) are state variables). The scaling of inputs is performed in the following way:

$$E = K_{\mathrm{d}}\eta\ ,\ EC = K_{\mathrm{v}}\dot{\eta}\ , \tag{13}$$

where E and EC present the error and the error derivative in the fuzzy set, respectively. The peak observer is constructed for each state variable and it monitors amplitudes and the increase of amplitudes of the state variable and calculates its rates. When the state variable reaches its peak, the corresponding scaling factor is tuning in the parameter regulator in a manner that input in the fuzzy logic controller is in the [-1 1] range. The objective function used in this issue is maximization of the ratio of the first ($\eta_{\max 1}$) and the second ($\eta_{\max 2}$) amplitude of the modal displacement:

$$OBJ_F = \text{maximize}\frac{\left|\eta_{\max 1}\right|}{\left|\eta_{\max 2}\right|} \tag{14}$$

However, increasing of the scaling factors during active vibration suppression results in the big and strong control force when the amplitude becomes too small, which can lead to control instability such as spillover. In order to overcome this problem, self-tuning FLC is combined with the LQR making the composite controller. The controller is switched from self-tuning FLC to LQR when the amplitude drops to 20% value of the maximum amplitude.

Numerical examples are provided for free vibration control of symmetric cantilever composite beam with layers orientation (90°/0°/90°/0°) and one integrated piezoelectric actuator for both single mode and multi-modal responses (first three modes). From these examples it can be inferred that the membership functions for both the Mamdani and the zero-order TSK inference method do not depend on the initial conditions and change of initial values of the scaling factors has very little impact on the control system performances. Comparing the PSO optimized self-tuning FLC with the FLC with constant factors and the LQR optimal control, it is found that proposed control algorithm leads to better vibration suppression. Also, the zero-order TSK inference method is more effective than the Mamdani inference method.

The goal of the paper is to adapt this PSO optimized self-tuning FLC for active vibration suppression of composite plates in the multiple-input multiple-output (MIMO) manner. Numerical simulation will be performed for the active vibration control of the first six modes of above presented cantilever symmetric, antisymmetric cross-ply and antisymmetric angle-ply composite plates with actuators configurations obtained by optimization. Unlike the case from paper [65], in this simulation the scaling factors will become constant when the amplitude drops to 20% value of the maximum amplitude (instead of switching on the LQR). A block diagram of the self-tuning FLC is presented in Figure 19, while Figure 20 presents a block diagram of the *i*-th modal subsystem (M. S. *i*). The optimization is performed for initial values obtained with impulse load of 500N with duration of 0.1ms at the point A of each plate (Figure 21). Initial values of the scaling factors are set to be zero ($K_d(0)=0,\ K_v(0)=0$). The maximum allowable voltage for each actuator is 200V ($K_{\mathrm{act}} = 200\mathrm{V}$). Optimization is performed for

each mode, independently, with all five actuators fully loaded. The number of population in PSO is 300 and the number of iterations is 500.

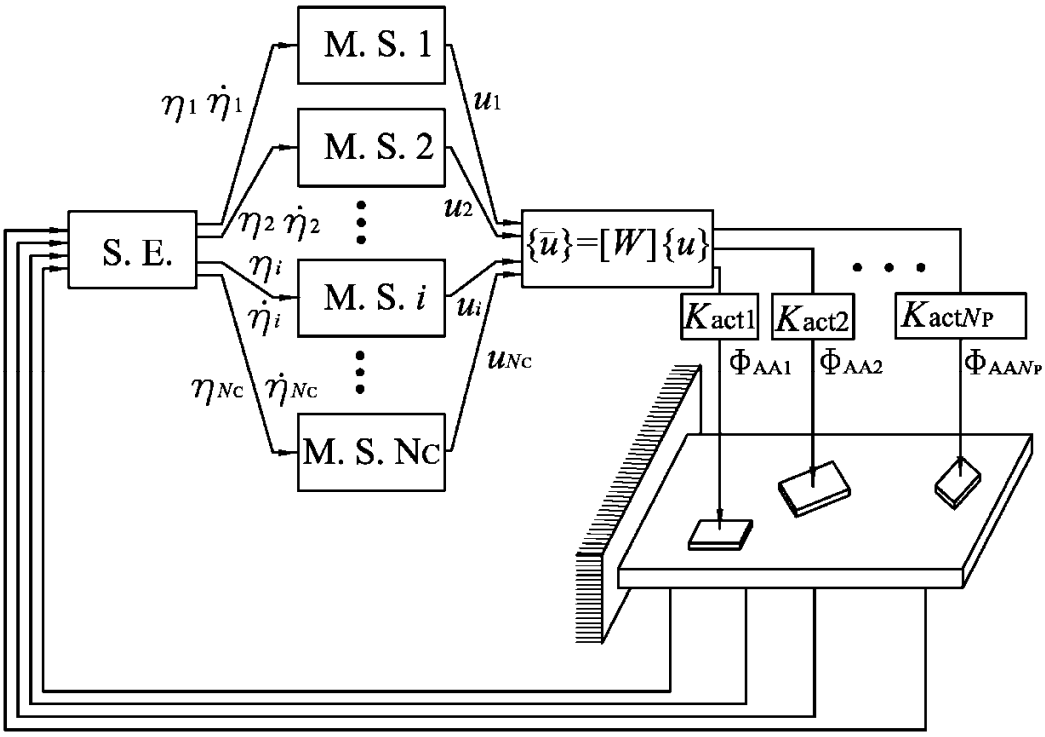

Fig. 19. Block diagram of self-tuning FLC (S. E. – State estimator; M. S. – Modal subsystem).

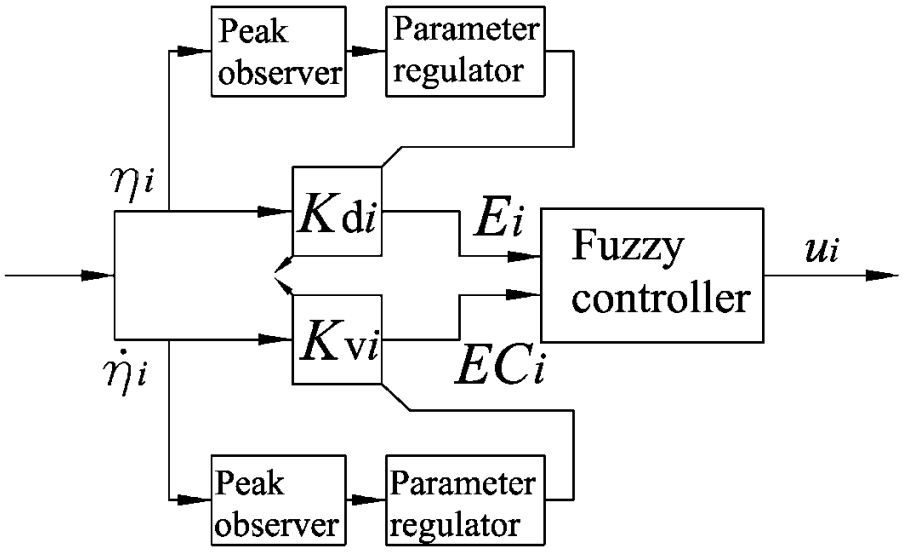

Fig. 20. Block diagram of the *i*-th modal subsystem (M. S. *i*).

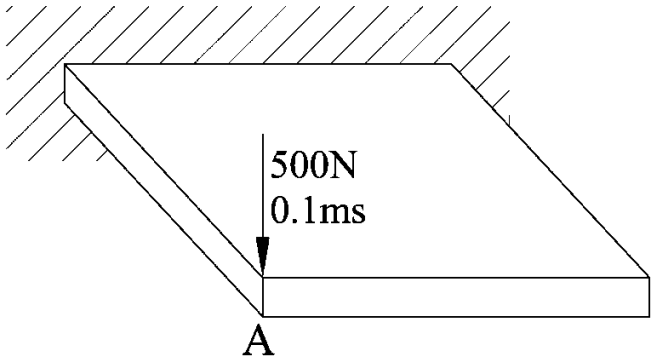

Fig. 21. Action of impulse load at the plate.

Obtained parameters α_i, β_i, γ_i and the objective function value of each mode for the Mamdani inference method are presented in Table 6. According to obtained parameters, the membership functions of inputs and output for this case are depicted in Fig. 22. Table 7 presents obtained parameters α_1, β_1 and the objective function value of each mode for the zero-order TSK inference method, while the membership functions of inputs are illustrated in Fig. 23. Analyzing parameters in Table 6 and Table 7, it can be inferred that the same corresponding parameters have the same value. In other words, obtained membership functions are the same for each mode and for each plate for both Mamdani and zero-order TSK inference methods. Comparing Table 6 with Tables 4 and 17 in paper [65], as well as Table 7 with Tables 14 and 18 in the same paper, it can be concluded that this membership functions have the same value for the first three modes in the case of Mamdani inference method and for the first two modes in the case of the zero-order TSK inference method. Also, obtained inference rules for each mode of each plate for the zero-order TSK inference method have the same value and they are presented in Table 8. Comparing Table 8 with Tables 15 and 19 in paper [65] it can be stated that the same values of inference rules are obtained.

Table 6
Optimized parameters α_i, β_i, γ_i and the objective function value (Obj.) of each mode for the self-tuning FLC based on the Mamdani inference method obtained by the PSO.

Symmetric plate						
Mode	1	2	3	4	5	6
$\begin{bmatrix}\alpha_1\\ \alpha_2\end{bmatrix}$	$\begin{bmatrix}1\\ 0.991\end{bmatrix}$	$\begin{bmatrix}1\\ 0.991\end{bmatrix}$	$\begin{bmatrix}1\\ 0.991\end{bmatrix}$	$\begin{bmatrix}1\\ 0.991\end{bmatrix}$	$\begin{bmatrix}1\\ 0.991\end{bmatrix}$	$\begin{bmatrix}1\\ 0.991\end{bmatrix}$
$\begin{bmatrix}\beta_1\\ \beta_2\end{bmatrix}$	$\begin{bmatrix}0.384\\ 0.278\end{bmatrix}$	$\begin{bmatrix}0.384\\ 0.278\end{bmatrix}$	$\begin{bmatrix}0.384\\ 0.278\end{bmatrix}$	$\begin{bmatrix}0.384\\ 0.278\end{bmatrix}$	$\begin{bmatrix}0.384\\ 0.278\end{bmatrix}$	$\begin{bmatrix}0.384\\ 0.278\end{bmatrix}$
$\begin{bmatrix}\gamma_1\\ \gamma_2\end{bmatrix}$	$\begin{bmatrix}1\\ 0.812\end{bmatrix}$	$\begin{bmatrix}1\\ 0.812\end{bmatrix}$	$\begin{bmatrix}1\\ 0.812\end{bmatrix}$	$\begin{bmatrix}1\\ 0.812\end{bmatrix}$	$\begin{bmatrix}1\\ 0.812\end{bmatrix}$	$\begin{bmatrix}1\\ 0.812\end{bmatrix}$
Obj.	1.1359	1.1114	1.125	1.091	1.0763	1.0786
Antisymmetric cross-ply plate						
Mode	1	2	3	4	5	6
$\begin{bmatrix}\alpha_1\\ \alpha_2\end{bmatrix}$	$\begin{bmatrix}1\\ 0.991\end{bmatrix}$	$\begin{bmatrix}1\\ 0.991\end{bmatrix}$	$\begin{bmatrix}1\\ 0.991\end{bmatrix}$	$\begin{bmatrix}1\\ 0.991\end{bmatrix}$	$\begin{bmatrix}1\\ 0.991\end{bmatrix}$	$\begin{bmatrix}1\\ 0.991\end{bmatrix}$
$\begin{bmatrix}\beta_1\\ \beta_2\end{bmatrix}$	$\begin{bmatrix}0.384\\ 0.278\end{bmatrix}$	$\begin{bmatrix}0.384\\ 0.278\end{bmatrix}$	$\begin{bmatrix}0.384\\ 0.278\end{bmatrix}$	$\begin{bmatrix}0.384\\ 0.278\end{bmatrix}$	$\begin{bmatrix}0.384\\ 0.278\end{bmatrix}$	$\begin{bmatrix}0.384\\ 0.278\end{bmatrix}$
$\begin{bmatrix}\gamma_1\\ \gamma_2\end{bmatrix}$	$\begin{bmatrix}1\\ 0.812\end{bmatrix}$	$\begin{bmatrix}1\\ 0.812\end{bmatrix}$	$\begin{bmatrix}1\\ 0.812\end{bmatrix}$	$\begin{bmatrix}1\\ 0.812\end{bmatrix}$	$\begin{bmatrix}1\\ 0.812\end{bmatrix}$	$\begin{bmatrix}1\\ 0.812\end{bmatrix}$
Obj.	1.1544	1.1136	1.2857	1.0716	1.076	1.0677
Antisymmetric angle-ply plate						
Mode	1	2	3	4	5	6
$\begin{bmatrix}\alpha_1\\ \alpha_2\end{bmatrix}$	$\begin{bmatrix}1\\ 0.991\end{bmatrix}$	$\begin{bmatrix}1\\ 0.991\end{bmatrix}$	$\begin{bmatrix}1\\ 0.991\end{bmatrix}$	$\begin{bmatrix}1\\ 0.991\end{bmatrix}$	$\begin{bmatrix}1\\ 0.991\end{bmatrix}$	$\begin{bmatrix}1\\ 0.991\end{bmatrix}$
$\begin{bmatrix}\beta_1\\ \beta_2\end{bmatrix}$	$\begin{bmatrix}0.384\\ 0.278\end{bmatrix}$	$\begin{bmatrix}0.384\\ 0.278\end{bmatrix}$	$\begin{bmatrix}0.384\\ 0.278\end{bmatrix}$	$\begin{bmatrix}0.384\\ 0.278\end{bmatrix}$	$\begin{bmatrix}0.384\\ 0.278\end{bmatrix}$	$\begin{bmatrix}0.384\\ 0.278\end{bmatrix}$
$\begin{bmatrix}\gamma_1\\ \gamma_2\end{bmatrix}$	$\begin{bmatrix}1\\ 0.812\end{bmatrix}$	$\begin{bmatrix}1\\ 0.812\end{bmatrix}$	$\begin{bmatrix}1\\ 0.812\end{bmatrix}$	$\begin{bmatrix}1\\ 0.812\end{bmatrix}$	$\begin{bmatrix}1\\ 0.812\end{bmatrix}$	$\begin{bmatrix}1\\ 0.812\end{bmatrix}$
Obj.	1.2165	1.0796	1.5994	1.0531	1.1023	1.2008

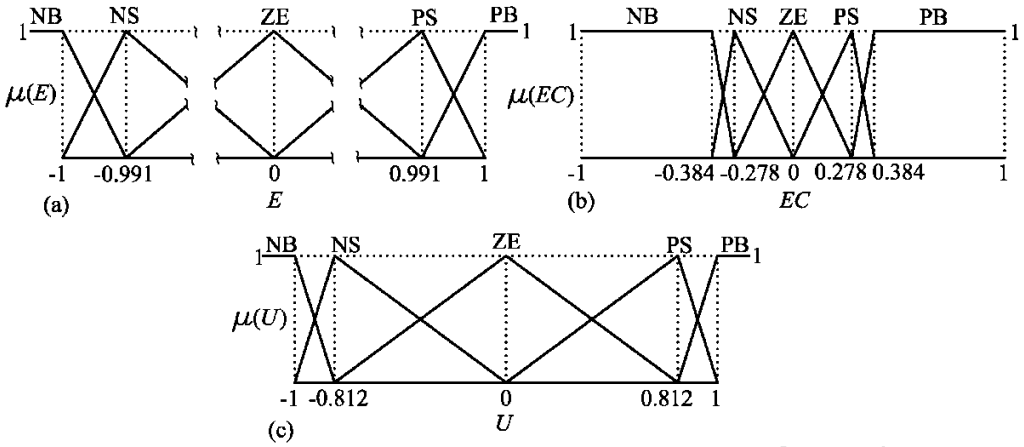

Fig. 22. Membership functions for the zero-order TSK inference method. (a) The input - error; (b) The input - error derivative; (c) The output.

Table 7

Optimized parameters α_1, β_1 and the objective function value (Obj.) of each mode for the self-tuning FLC based on the zero-order TSK inference method obtained by the PSO.

Symmetric plate						
Mode	1	2	3	4	5	6
α_1	1	1	1	1	1	1
β_1	0.16	0.16	0.16	0.16	0.16	0.16
Obj.	1.2804	1.222	1.2559	1.1721	1.1397	1.1459
Antisymmetric cross-ply plate						
Mode	1	2	3	4	5	6
α_1	1	1	1	1	1	1
β_1	0.16	0.16	0.16	0.16	0.16	0.16
Obj.	1.3268	1.2271	1.7157	1.1354	1.1397	1.1314
Antisymmetric angle-ply plate						
Mode	1	2	3	4	5	6
α_1	1	1	1	1	1	1
β_1	0.16	0.16	0.16	0.16	0.16	0.16
Obj.	1.4982	1.1514	3.3392	1.0972	1.2004	1.4638

Table 8
Inference rules of each mode for the self-tuning FLC based on the zero-order TSK inference method obtained by the PSO.

Symmetric plate						
		EC				
		NB	NS	ZE	PS	PB
E	NB	1	1	0.992	0.259	0.183
	NS	0.979	0.221	0.22	-0.247	-0.519
	ZE	0.953	0.282	0	-0.282	-0.953
	PS	0.519	0.247	-0.22	-0.221	-0.979
	PB	-0.183	-0.259	-0.992	-1	-1
Antisymmetric cross-ply plate						
		EC				
		NB	NS	ZE	PS	PB
E	NB	1	1	0.992	0.259	0.183
	NS	0.979	0.221	0.22	-0.247	-0.519
	ZE	0.953	0.282	0	-0.282	-0.953
	PS	0.519	0.247	-0.22	-0.221	-0.979
	PB	-0.183	-0.259	-0.992	-1	-1
Antisymmetric angle-ply plate						
		EC				
		NB	NS	ZE	PS	PB
E	NB	1	1	0.992	0.259	0.183
	NS	0.979	0.221	0.22	-0.247	-0.519
	ZE	0.953	0.282	0	-0.282	-0.953
	PS	0.519	0.247	-0.22	-0.221	-0.979
	PB	-0.183	-0.259	-0.992	-1	-1

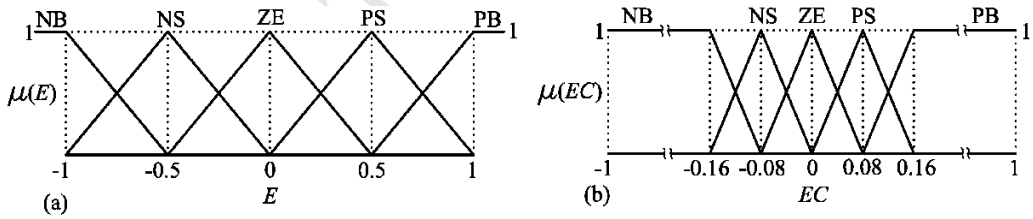

Fig. 23. Membership functions for Mamdani inference method. (a) The input - error; (b) The input - error derivative.

6.1 Optimization of output matrix for MIMO application

Since optimization is performed for each mode independently with fully loaded actuators, fully loaded actuators for each mode in simultaneous control of the first six modes cannot be applied because maximum applied voltage will exceed 200V, which leads to depolarization of PZT material. Therefore, it is necessary to select the output matrix ($[W]$). In this paper this matrix will be found by using the PSO algorithm. The objective function is defined as

$$OBJ_W = \text{maximize}\left(\min_{i=1,..,6} \left(\frac{\left(\left|\eta_{\max 1}\right| / \left|\eta_{\max 2}\right| \right)_i}{\left(\left|\eta_{\max 1}\right| / \left|\eta_{\max 2}\right| \right)_{\max i}} \right) \right), \tag{15}$$

where $\left(\left|\eta_{\max 1}\right| / \left|\eta_{\max 2}\right| \right)_i$ presents the ratio of the first and the second amplitude of modal displacement of the i-th mode, while $\left(\left|\eta_{\max 1}\right| / \left|\eta_{\max 2}\right| \right)_{\max i}$ presents the maximum ratio of the first and the second amplitude of modal displacement of the i-th mode obtained when all actuators are fully loaded (these values are given in Tables 6 and 7). Constraints are regarded to the maximum applied voltage at the actuator

$$\left|\Phi_{\mathrm{AA}j}\right|_{\max} \le 200\mathrm{V}, \quad j=1,\ldots,5\,. \tag{16}$$

Considering defined constraints, the objective function can be written as

$$OBJ_W = \text{maximize}\left(J_W\right),$$

$$J_W = \begin{cases} \min_{i=1,..,6} \left(\dfrac{\left(\left|\eta_{\max 1}\right| / \left|\eta_{\max 2}\right| \right)_i}{\left(\left|\eta_{\max 1}\right| / \left|\eta_{\max 2}\right| \right)_{\max i}} \right), & \text{if constraints are not violated} \\ 0, & \text{if any of the constraints is violated} \end{cases}. \tag{17}$$

According to the optimization statements, the i-th particle in the k-th iteration is defined by the following coordinates

$$\left[p_i^k \right] = \left[W_{mn\,i}^k \right], \quad m=1,\ldots,6, \quad n=1,\ldots 5\,. \tag{18}$$

In order to increase computation effectiveness, initial population is generated by setting their range according to the matrix $\left[\bar{B}\right]$ that is presented in Table 9 for each configuration of plates. According to the values in these matrices, the initial population is chosen in the way in which a larger value of controllability of a particular mode by a particular actuator implies a larger value of corresponding member of the output matrix $[W]$. The initial values for each configuration of plates are presented in Table 10. Obtained values are shown in the next subsection, where control performances of the PSO-optimized fuzzy logic control will be analyzed.

Table 9
Matrix $\left[\bar{B}\right]$ for each configuration of plates.

	$\left[\bar{B}\right]\left(\times 10^{-3}\right)$				
Symmetric plate	−1.7234	−1.7864	0.0636	−0.4109	−0.1088
	3.4777	−3.2990	0.0205	1.9786	−1.7422
	−7.7103	−7.0136	−2.1983	4.9142	1.1116
	−10.9496	11.8344	0.3721	6.5562	−8.2981
	2.7150	2.9872	27.0033	5.4953	5.5988
	11.1649	12.5939	−23.7795	−4.3202	−14.7885
Antisymmetric cross-ply plate	2.5132	2.4353	0.0999	0.4431	−0.3381
	−4.3612	4.3648	−0.0344	−1.6662	−1.3873
	9.6353	9.9712	−6.0049	−5.4275	0.6359
	2.7837	1.9586	−25.4528	4.8027	−3.3711
	−13.9086	14.2546	−1.2840	6.5760	−1.4028
	−13.7066	−13.3055	−23.8801	−0.5615	6.9218
Antisymmetric angle-ply plate	−1.6125	−1.4463	0.2107	−1.4508	−0.4805
	4.6956	−4.8513	−0.3166	−0.8696	0.4298
	−8.4390	−9.0663	−3.5493	8.8357	7.9166
	0.8639	−0.3404	−15.8909	−4.7568	2.0950
	−12.5398	14.1052	−1.9419	13.8924	−4.8362
	16.2911	17.5060	1.3064	−19.2859	26.9088

Table 10
Initial values of output matrix $[W]$ for each configuration of plates.

	Initial $[W]$
Symmetric plate	$\begin{bmatrix} 0.4-0.8 & 0.4-0.8 & 0 & 0-0.1 & 0 \\ 0.3-0.7 & 0.3-0.7 & 0 & 0.1-0.5 & 0.2-0.3 \\ 0-0.2 & 0-0.2 & 0-0.1 & 0.4-0.5 & 0.1-0.3 \\ 0.1-0.2 & 0.1-0.2 & 0 & 0.1-0.4 & 0.5-0.8 \\ 0-0.1 & 0-0.1 & 0.4-0.7 & 0.2-0.4 & 0.1-0.3 \\ 0-0.2 & 0-0.2 & 0.4-0.7 & 0 & 0.1-0.5 \end{bmatrix}$
Antisymmetric cross-ply plate	$\begin{bmatrix} 0.3-0.7 & 0.3-0.7 & 0 & 0.1-0.3 & 0 \\ 0.3-0.7 & 0.3-0.7 & 0 & 0-0.3 & 0.1-0.5 \\ 0-0.3 & 0-0.3 & 0-0.1 & 0.5-0.8 & 0-0.1 \\ 0-0.1 & 0-0.1 & 0.5-1 & 0-0.2 & 0.1-0.4 \\ 0.1-0.3 & 0.1-0.3 & 0 & 0.1-0.3 & 0-0.5 \\ 0.1-0.2 & 0.1-0.2 & 0.3-0.6 & 0 & 0.3-0.7 \end{bmatrix}$
Antisymmetric angle-ply plate	$\begin{bmatrix} 0.4-0.7 & 0.4-0.7 & 0 & 0.1-0.3 & 0 \\ 0.3-0.8 & 0.3-0.8 & 0 & 0-0.2 & 0 \\ 0-0.5 & 0-0.5 & 0.4-0.7 & 0.3-0.6 & 0.3-0.6 \\ 0 & 0 & 0.5-1 & 0.1-0.3 & 0-0.2 \\ 0.1-0.3 & 0.1-0.3 & 0 & 0.2-0.7 & 0.1-0.5 \\ 0.1-0.4 & 0.1-0.4 & 0 & 0.3-0.7 & 0.4-0.8 \end{bmatrix}$

7. Active vibration control analysis

Obtained values for the output matrix $[W]$ as well as the maximum applied control voltages on each actuator are presented in Table 11 for the symmetric plate for both Mamdani and zero-order TSK inference method. In order to compare the optimized self-tuning FLC with one of the most used conventional controllers – LQR, the weighting matrices $[Q]$ and $[R]$ are found using the trial and error method keeping maximum applied control voltages to the actuators below 200 V. These matrices along with maximum applied control voltages are also presented in Table 11. These results for antisymmetric cross-ply and angle-ply composite plates are given as supplementary material. In all cases the scaling factors become constant when the amplitude drops to 20% value of the maximum amplitude.

Table 11

Optimized output matrix $[W]$ for the Mamdani and the TSK inference methods, matrices $[Q]$ and $[R]$ for the LQR control and maximum applied control voltage for the symmetric composite plate.

Mamdani

$$[W]=\begin{bmatrix} 0.7296 & 0.7602 & 0 & 0.0019 & 0 \\ 0.582 & 0.61 & 0 & 0.4395 & 0.2143 \\ 0.1194 & 0.1258 & 0.0978 & 0.4351 & 0.2374 \\ 0.1826 & 0.1909 & 0 & 0.3697 & 0.7805 \\ 0.0442 & 0.0448 & 0.5817 & 0.386 & 0.2323 \\ 0.022 & 0.0245 & 0.6491 & 0 & 0.4286 \end{bmatrix}$$

$$|\Phi_{AA1}|_{max}=200.00\text{V}$$
$$|\Phi_{AA2}|_{max}=200.00\text{V}$$
$$|\Phi_{AA3}|_{max}=199.80\text{V}$$
$$|\Phi_{AA4}|_{max}=197.13\text{V}$$
$$|\Phi_{AA5}|_{max}=198.54\text{V}$$

TSK

$$[W]=\begin{bmatrix} 0.4973 & 0.4595 & 0 & 0.0649 & 0 \\ 0.3832 & 0.354 & 0 & 0.1153 & 0.321 \\ 0.0229 & 0.0212 & 0.0116 & 0.4801 & 0.1288 \\ 0.1124 & 0.1039 & 0 & 0.1644 & 0.5049 \\ 0 & 0 & 0.4976 & 0.2246 & 0.1335 \\ 0.1108 & 0.1005 & 0.4975 & 0 & 0.1374 \end{bmatrix}$$

$$|\Phi_{AA1}|_{max}=200.00\text{V}$$
$$|\Phi_{AA2}|_{max}=199.87\text{V}$$
$$|\Phi_{AA3}|_{max}=199.82\text{V}$$
$$|\Phi_{AA4}|_{max}=199.97\text{V}$$
$$|\Phi_{AA5}|_{max}=200.00\text{V}$$

LQR

$$[Q]=10^6[\mathrm{I}]_{12\times12} \qquad [R]=\begin{bmatrix} 1.6 & 0 & 0 & 0 & 0 \\ 0 & 1.5 & 0 & 0 & 0 \\ 0 & 0 & 2.2 & 0 & 0 \\ 0 & 0 & 0 & 1.5 & 0 \\ 0 & 0 & 0 & 0 & 1 \end{bmatrix}$$

$$|\Phi_{AA1}|_{max}=197.33\text{V}$$
$$|\Phi_{AA2}|_{max}=199.75\text{V}$$
$$|\Phi_{AA3}|_{max}=197.88\text{V}$$
$$|\Phi_{AA4}|_{max}=200.00\text{V}$$
$$|\Phi_{AA5}|_{max}=198.45\text{V}$$

Comparison of control performance of the PSO optimized self-tuning FLC based on the Mamdani and zero-order TSK inference methods and the LQR optimal control for the symmetric composite plate is presented in Figure 24, where the displacement history of the point A for multimodal response of the plate is depicted. Figure 25 shows a single-mode response of the point A for each controlled mode. It can be inferred from Figure 24 that the PSO-optimized self-tuning FLC leads to better vibration suppression compared to LQR optimal control and the zero-order TSK inference method has better performances than the Mamdani inference method. The same conclusion can be drawn from Figure 25, especially for lower modes (1^{st} and 2^{nd}). For higher modes (3^{rd} – 6^{th}), LQR optimal control provides lower amplitudes at the beginning of vibration suppression, but it also provides higher settling time. Control voltages in the

multimodal response of each actuator for each control algorithm, as well as deflection of point A of the antisymmetric cross-ply and angle-ply composite plates are given as supplementary material.

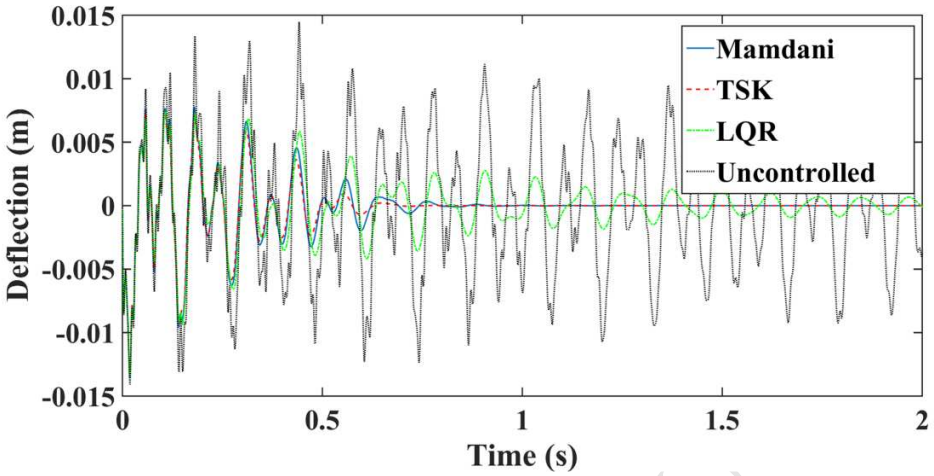

Fig. 24. Deflection of point A of the symmetric composite plate for the multimodal response.

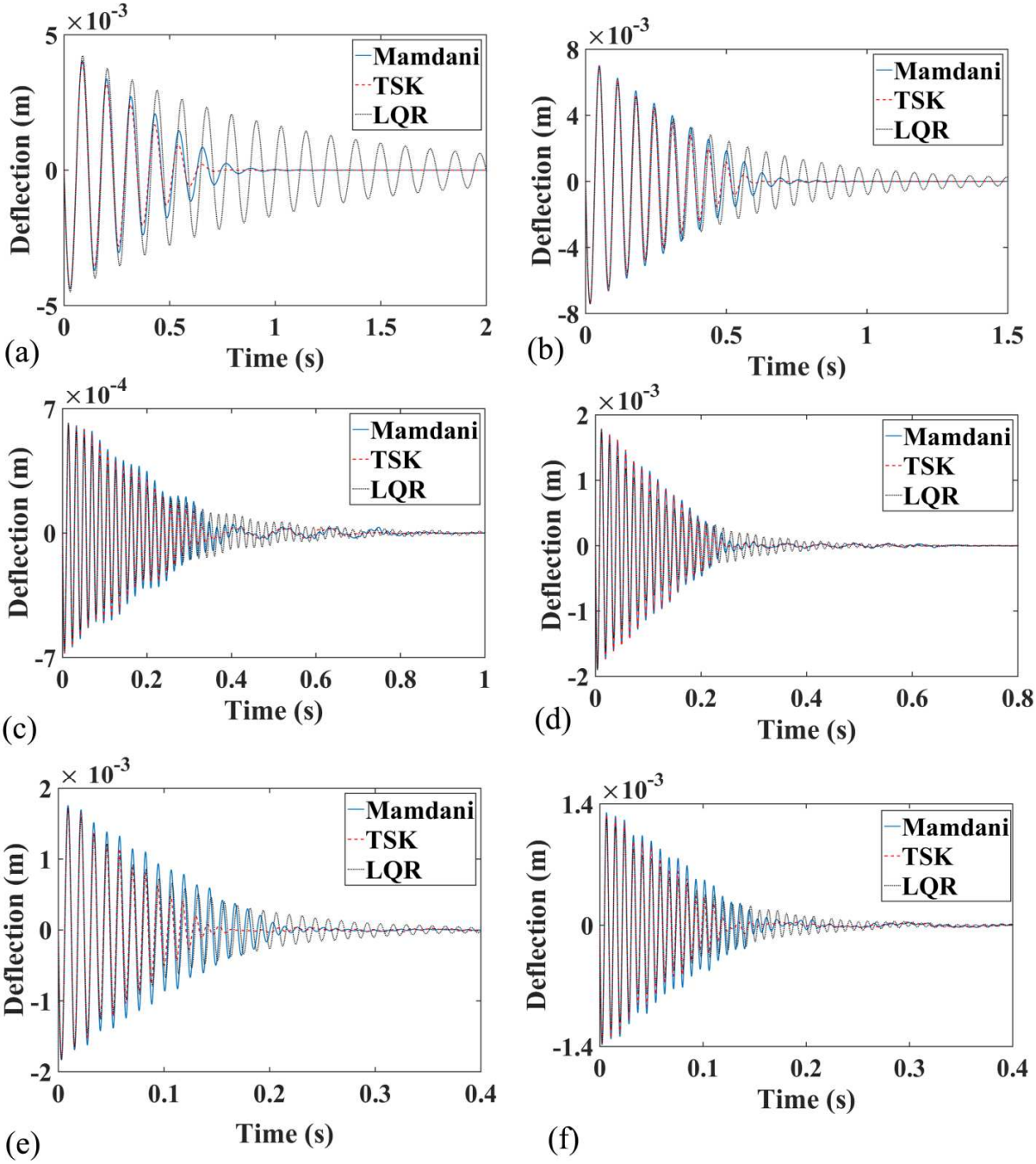

Fig. 25. Deflection of point A of the symmetric composite plate for the single mode responses: (a) 1st mode, (b) 2nd mode, (c) 3rd mode, (d) 4th mode, (e) 5th mode and (f) 6th mode.

8. Optimization procedure: summary

The optimization procedure presented in this paper can be summarized using the flowchart as illustrated by Figure 26.

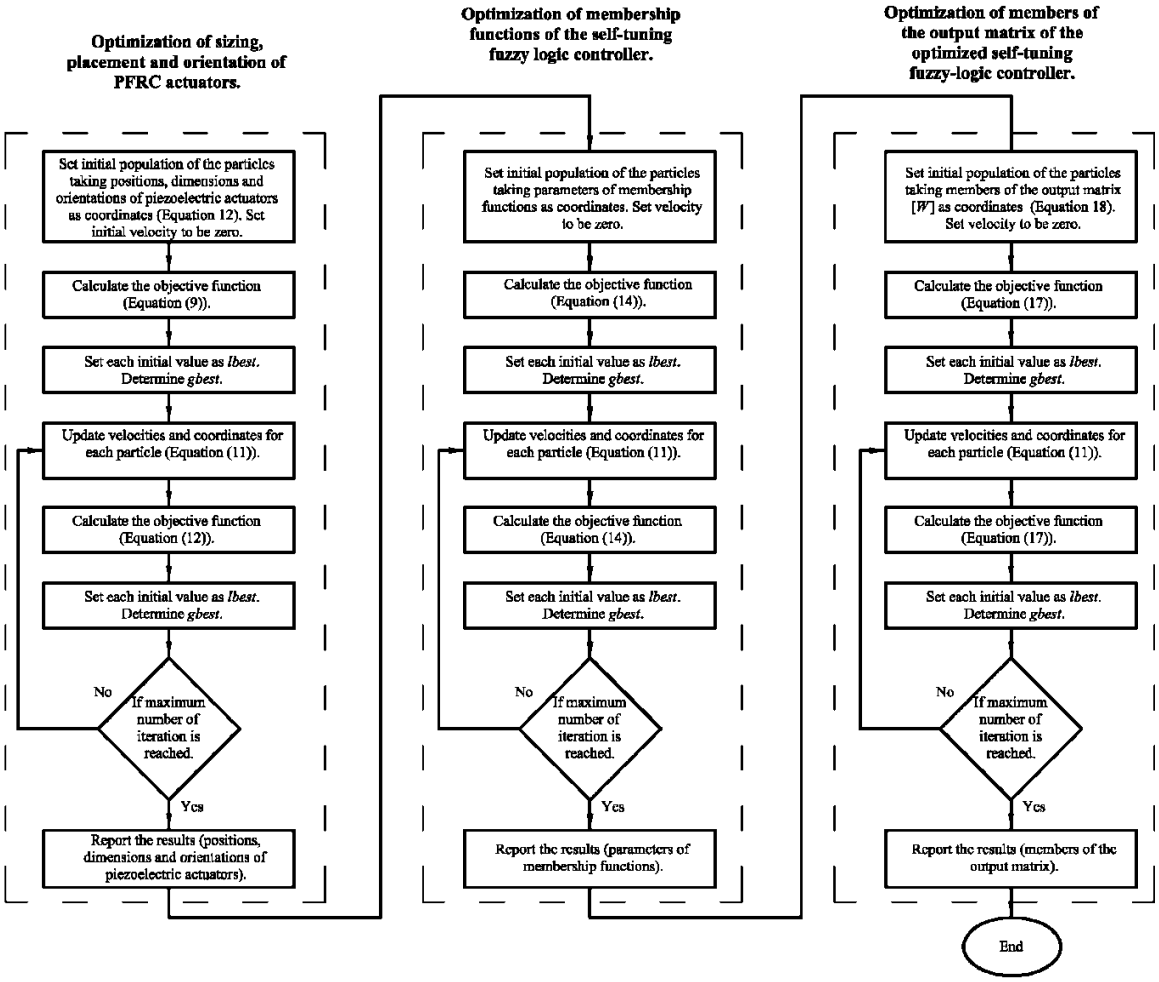

Fig. 26. Flowchart of the optimization procedure.

9. Conclusions

In this paper, optimization of the sizing, location and orientation of PFRC actuators and the active vibration control of smart composite plates using the particle-swarm optimized self-tuning fuzzy logic controller is studied. Numerical analysis is performed for active vibration control of the first six modes of the cantilever symmetric $((90°/0°/90°/0°)_S)$, antisymmetric cross-ply ((90°/0°/90°/0°/90°/0°/90°/0°)) and antisymmetric angle-ply ((45°/-45°/45°/-45°/45°/-45°/45°/-45°)) composite plates.

The analysis of influence of the PFRC actuator layer orientation and position (top or bottom side of the plates) on the Gramian controllability matrix shows that there is a significant difference, depending on whether the actuator is placed on the top or the bottom side of the antisymmetric plates. The reason is the presence of the bending-extension coupling stiffnesses in this type of laminates. It can be concluded that higher controllability is achieved in the case when the actuator is placed on the side where the angle between the actuator fibers and fibers of the layer in contact has a larger value. The experimental study is performed in order to validate such behavior of antisymmetric plate. This fact is taken into account for

optimization of the sizing, location and orientation of five PFRC actuators, which is also performed in the paper. Optimal configurations are found by using the PSO algorithm that involves the limitation of the plates masses increase.

Optimization of the membership functions parameters of the self-tuning fuzzy logic controller is performed by applying PSO algorithm for each mode of each plate independently for both the Mamdani and the zero-order Takagi–Sugeno–Kang fuzzy inference methods. Comparing the obtained membership functions, it can be concluded that they do not depend on controlled mode and plate configuration. In other words, the membership functions of certain input or output are equal for each mode of each plate, although they do not have the same material characteristic (because of layers orientations) or the positions, sizes and orientations of actuators. Also, they are equal to corresponding membership functions obtained for active vibration control of cantilever composite beam presented in [65], although they are a different type of structures, and optimization is performed under different initial conditions and different initial values of the scaling factors. Considering these facts, it is arrived at the conclusion that one of the main problems that occurs in the FLC design has been overcome by using the presented algorithm: tuning of the membership functions, especially in the cases when material and loading characteristics of the structures can be determined exactly. Furthermore, the output matrices are found by applying the particle swarm optimization. Also, it is found that the proposed control algorithm shows better performances and leads to better vibration suppression compared to LQR optimal control.

Further step involves implementation of the presented control algorithm for active vibration control in more complex and real structures, as well as experimental investigation.

Acknowledgment

This work is supported by the Ministry of Science and Technological Development of Republic of Serbia through Technological Development Project no. 35035.

8. References

[1] J.W. High, W.K. Wilkie, Method of fabricating NASA-standard Macro-Fiber Composite piezoelectric actuators, Technical Report NASA/TM-2003-212427, ARL-TR-2833. NASA Langley Research Center, Hampton, VA, USA, (2003). https://ntrs.nasa.gov/archive/nasa/casi.ntrs.nasa.gov/20030063125.pdf

[2] N.D. Zorić, A.M. Simonović, Z.S. Mitrović, S.N. Stupar, Optimal vibration control of smart composite beams with optimal size and location of piezoelectric sensing and actuation, J. Int. Mat. Sys. Struct. 24 (2013) 499-526. https://doi.org/10.1177/1045389X12463465

[3] V.Gupta, M.Sharma, N.Thakur, Optimization Criteria for Optimal Placement of Piezoelectric Sensors and Actuators on a Smart Structure: A Technical Review, J. Int. Mat. Sys. Struct. 21 (2010) 1227-1243. https://doi.org/10.1177/1045389X10381659

[4] K.R. Kumar, S. Narayanan, The optimal location of piezoelectric actuators and sensors for vibration control of plates, Smart Mat. Struct. 16 (2007) 2680-2691. https://doi.org/10.1088/0964-1726/16/6/073

[5] N. Darivandi, K.Morris, A.Khajepour, An algorithm for LQ optimal actuator location, Sm. Mat. Struct. 22 (2013) 035001 (1-10). https://doi.org/10.1088/0964-1726/22/3/035001

[6] F. Peng, A. Ng, Y.R. Hu, Actuator placement optimization and adaptive vibration control of plate smart structures, J. Int. Mat. Sys. Struct. 16 (2005) 263-271. https://doi.org/10.1177/1045389X05050105

[7] J.-H. Han, I. Lee, Optimal placement of piezoelectric sensors and actuators for vibration control of a composite plate using genetic algorithms, Smart Mat. Struct. 8 (1999) 257-267. https://doi.org/10.1088/0964-1726/8/2/012

[8] X. Liu, G. Cai, F. Peng, H. Zhang, Piezoelectric Actuator Placement Optimization and Active Vibration Control of a Membrane Structure, Acta Mech. Solida Sin. 31 (2018). https://doi.org/10.1007/s10338-018-0005-y

[9] D. Halim, S.O.R. Moheimani, An optimization approach to optimal placement of collocated piezoelectric actuators and sensors on a thin plate, Mechatronics. 13 (2003) 27-47. https://doi.org/10.1016/S0957-4158(01)00079-4

[10] T. Nestorović, M. Trajkov, Optimal actuator and sensor placement based on balanced reduced models, Mech. Sys. Sign. Proc. 36 (2013) 271–289. https://doi.org/10.1016/j.ymssp.2012.12.008

[11] D. Chhabra, G. Bhushan, P. Chandna, Optimal placement of piezoelectric actuators on plate structures for active vibration control via modified control matrix and singular value decomposition approach using modified heuristic genetic algorithm, Mech. Adv. Mat. Struct. 23 (2016) 272-280. https://doi.org/10.1080/15376494.2014.949932

[12] T.H. Quoc, V.V. Tham, T.M. Tu, Optimal placement and active vibration control of composite plates integrated piezoelectric sensor/actuator pairs, Viet. J. of Sc. Techn. 56 (2018) 113-126. https://doi.org/10.15625/2525-2518/56/1/8824

[13] A.H. Daraji, J.M. Hale, J. Ye, New methodology for optimal placement of piezoelectric sensor/actuator pairs for active vibration control of flexible structures, J. V. Acous. 140 (2018) 011015 (1-13). https://doi.org/10.1115/1.4037510

[14] V.M.F. Correia, C.M.M. Soares, C.A.M. Soares, Refined models for the optimal design of adaptive structures using simulated annealing, Comp. Struct. 54 (2001) 161-167. https://doi.org/10.1016/S0263-8223(01)00085-X

[15] Z.-G. Song, F.-M. Li, E. Carrera, P. Hagedorn, A new method of smart and optimal flutter control for composite laminated panels in supersonic airflow under thermal effects, J. Sound Vib. 414 (2018) 218-232. https://doi.org/10.1016/j.jsv.2017.11.008

[16] A.M. Simonović, M.M. Jovanović, N.S. Lukić, N.D. Zorić, S.N. Stupar, S.S. Ilić, Experimental studies on active vibration control of smart plate using a modified PID controller with optimal orientation of piezoelectric actuator, J. Vib. Cont. 22 (2016) 2619–2631. https://doi.org/10.1177/1077546314549037

[17] P. Kedziora, A. Muc, Optimal shapes of PZT actuators for laminated structures subjected to displacement or eigenfrequency constraints, Comp. Struct. 94 (2012) 1224–1235. https://doi.org/10.1016/j.compstruct.2011.11.019

[18] Q.Wang, C.M. Wang, Optimal placement and size of piezoelectric patches on beams from the controllability perspective, Smart Mat. Struct. 9 (2000) 558-567. https://doi.org/10.1088/0964-1726/9/4/320

[19] S.T. Quek, S.Y. Wang, K.K. Ang, Vibration Control of Composite Plates via Optimal Placement of Piezoelectric Patches, J. Int. Mat. Sys. Struct. 14 (2013) 229-245. https://doi.org/10.1177/1045389X03034686

[20] I. Bruant, L. Gallimard, S. Nikoukar, Optimal piezoelectric actuator and sensor location for active vibration control using genetic algorithm, J. Sound Vib. 329 (2010) 1615-1635. https://doi.org/10.1016/j.jsv.2009.12.001

[21] B. Yassin, A. Lahcen, E.-S.M. Zeriab, Hybrid optimization procedure applied to optimal location finding for piezoelectric actuators and sensors for active vibration control, Appl. Math. Mod. 62 (2018) 701-716. https://doi.org/10.1016/j.apm.2018.06.017

[22] Z.C. Qiu, X.M. Zhang, H.X. Wu, H.H. Zhang, Optimal placement and active vibration control for piezoelectric smart flexible cantilever plate, J. Sound Vib. 301 (2007) 521-543. https://doi.org/10.1016/j.jsv.2006.10.018

[23] P. Ambrosio, F. Resta, F. Ripamonti, An H_2 norm approach for the actuator and sensor placement in vibration control of a smart structure, Smart Mat. Struct. 21 (2012) 125016 (1-11). https://doi.org/10.1088/0964-1726/21/12/125016

[24] M. Biglar, H.R. Mirdamadi, Integrated and consistent active control formulation and piezotransducer position optimization of plate structures considering spillover effects, Shock Vib. 2014, Article ID 276714 1-14. http://dx.doi.org/10.1155/2014/276714

[25] A. Montazeri, J. Poshtan, A. Yousefi-Koma, The use of “particle swarm” to optimize the control system in a PZT laminated plate, Smart Mat. Struct. 17 (2008) 045027 (1-7). https://doi.org/10.1088/0964-1726/17/4/045027

[26] G.A. Foutsitzi, C.G. Gogos, E.P. Hadjigeorgiou, G.E. Stavroulakis, Actuator Location and Voltages Optimization for Shape Control of Smart Beams Using Genetic Algorithms, Actuators, 2 (2013) 111-128. https://doi.org/10.3390/act2040111

[27] Y. Jingyu, C. Guoping, Multi-objective optimization of orientations and locations of actuators and sensors for structural shape control, Adv. Sc. Lett. 6 (2012), 511-517. https://doi.org/10.1166/asl.2012.2197

[28] Y. Jingyu, C. Guoping, Orientations and locations optimization of actuators and sensors for structural shape control, Adv. Sc. Lett. 6 (2012), 547-552. https://doi.org/10.1166/asl.2012.2239

[29] K. Yang, J. Zhu, M. Wu, W. Zhang, Integrated optimization of actuators and structural topology of piezoelectric composite structures for static shape control, Comput. Methods Appl. Mech. Engrg. 334 (2018) 440–469. https://doi.org/10.1016/j.cma.2018.01.021

[30] M.S. Azzouz, C. Mei, J.S. Bevan, J.J. Ro, Finite element modeling of MFC/AFC actuators and performance of MFC, J. Int. Mat. Sys. Struct. 12 (2001) 601-612. https://doi.org/10.1177/10453890122145384

[31] S. Kapuria, M.Y. Yasin, Active vibration suppression of multilayered plates integrated with piezoelectric fiber reinforced composites using an efficient finite element model, J. Sound Vib. 329 (2010) 3247-3265. https://doi.org/10.1016/j.jsv.2010.02.019

[32] S. Kapuria, M.Y. Yasin, Active vibration control of smart plates using directional actuation and sensing capability of piezoelectric composites, Acta Mech. 224 (2013), 1185–1199. https://doi.org/10.1007/s00707-013-0864-8

[33] J. Li, F. Li, Y. Narita, Active control of thermal buckling and vibration for a sandwich composite laminated plate with piezoelectric fiber-reinforced composite actuator facesheets, J. Sandw. Struct. Mater. Accepted article (2018). https://doi.org/10.1177/1099636218783168

[34] S. Gohari, S. Sharifi, R. Abadi, M. Izadifar, C. Burvill, Z. Vrcelj, A quadratic piezoelectric multi-layer shell element for FE analysis of smart laminated composite plates induced by MFC actuators. Smart Mat. Struct. 27 (2018) 095004 1-39. https://doi.org/10.1088/1361-665X/aacc95

[35] X. Wang, W. Zhou, Z. Wu, W. Wu, Optimal unimorph and bimorph configurations of piezocomposite actuators for bending and twisting vibration control of plate structures, J. Int. Mat. Sys. Struct. 29 (2018) 1685–1696. https://doi.org/10.1177/1045389X17742736

[36] S.Y. Wang, S.T. Quek, K.K. Ang, Dynamic stability analysis of finite element modeling of piezoelectric composite plates, Int. J. Sol. Struct. 41 (2004) 745-764. https://doi.org/10.1016/j.ijsolstr.2003.09.041

[37] S. Narayanan, V. Balamurugan, Finite element modelling of piezolaminated smart structures for active vibration control with distributed sensors and actuators, J. Sound Vib. 262 (2003) 529-562. https://doi.org/10.1016/S0022-460X(03)00110-X

[38] S.J. Lee, J.N. Reddy, F. Rostam-Abadi, Transient analysis of laminated composite plates with embedded smart-materials layers, Fin. Elem. Analy. Des. 40 (2004) 463-483. https://doi.org/10.1016/S0168-874X(03)00073-8

[39] X. Zhang, Z. Kang, Topology optimization of piezoelectric layers in plates with active vibration control, J. Int. Mat. Sys. Struct. 25 (2014) 697–712. https://doi.org/10.1177/1045389X13500577

[40] Z.G. Song, L.W. Zhang, K.M. Liew, Active vibration control of CNT reinforced functionally graded plates based on a higher-order shear deformation theory, Int. J. Mech. Sc. 105 (2016) 90–101. https://doi.org/10.1016/j.ijmecsci.2015.11.019

[41] X. Zhang, A. Takezawa, Z. Kang, Topology optimization of piezoelectric smart structures for minimum energy consumption under active control, Struct. Multidisc. Opt. 58 (2018) 185–199. https://doi.org/10.1007/s00158-017-1886-y

[42] M.M Jovanović, A.M. Simonović, N. D. Zorić, N.S. Lukić, S.N. Stupar, S.S. Ilić, Experimental studies on active vibration control of a smart composite beam using a PID controller, Smart Mat. Struct. 22 (2013) 115038 1-8. https://doi.org/10.1088/0964-1726/22/11/115038

[43] Y. Li, X. Wang, R. Huang, Z. Qiu, Active vibration and noise control of vibro-acoustic system by using PID controller, J. Sound Vib. 348 (2015) 57–70. https://doi.org/10.1016/j.jsv.2015.03.017

[44] M. Ezzraimi, R. Tiberkak, A. Melbous, S. Rechak, LQR and PID Algorithms for Vibration Control of Piezoelectric Composite Plates, Mech. 24 (2018) 734-740. http://dx.doi.org/10.5755/j01.mech.24.5.20645

[45] I. R. Birs, C. I. Muresan, S. Folea, O. Prodan, A Comparison between integer and fractional order PD^{μ} controllers for vibration suppression, App. Math. Nonlin. Sc. 1 (2016) 273–282, https://doi.org/10.21042/AMNS.2016.1.00022

[46] S. Folea, R.D. Keyser, I.R. Birs, C.I. Muresan, C. Ionescu, Discrete-time implementation and experimental validation of a fractional order PD controller for vibration suppression in airplane wings, Acta Polytechn. Hun. 14 (2017) 191-206. https://doi.org/10.12700/APH.14.1.2017.1.13

[47] C.I. Muresan, S. Folea, I.R. Birs, C. Ionescu, A novel fractional-order model and controller for vibration suppression in flexible smart beam, Non. Dyn. 93 (2018), 525–541. https://doi.org/10.1007/s11071-018-4207-0

[48] L. Marinangeli, F. Alijani, S.H.H. Nia, Fractional-order positive position feedback compensator for active vibration control of a smart composite plate. J. Sound Vib. 412 (2018) 1–16. https://doi.org/10.1016/j.jsv.2017.09.009

[49] X.J. Dong, G. Meng, J.C. Peng, Vibration control of piezoelectric smart structures based on system identification technique: numerical simulation and experimental study, J. Sound Vib. 297 (2006) 680–693. https://doi.org/10.1016/j.jsv.2006.04.021

[50] X. Dong, L. Ye, Z. Peng, H. Hua, G. Meng, A study on controller structure interaction of piezoelectric smart structures based on finite element method, J. Int. Mat. Sys. Struct. 25 (2014) 1401–1413. https://doi.org/10.1177/1045389X13507353

[51] O.A.A. Silveira, J.S.O. Fonseca, I.F. Santos, Actuator topology design using the controllability Gramian, Struct. Multidisc. Optim. 51 (2015) 145–157. https://doi.org/10.1007/s00158-014-1121-z

[52] E. Padoin, J.S.O. Fonseca, E.A. Perondi, O. Menuzzi, Optimal placement of piezoelectric macro fiber composite patches on composite plates for vibration suppression, Lat. Amer. J. Sol. Struct. 12 (2015) 925-947. http://dx.doi.org/10.1590/1679-78251320

[53] J.F. Gonçalves, D.M. De Leon, E.A. Perondi, Topology optimization of embedded piezoelectric actuators considering control spillover effects, J. Sound Vib. 388 (2017) 20–41. http://dx.doi.org/10.1016/j.jsv.2016.11.001

[54] M.D.F. Awruch, H.M. Gomes, A fuzzy α-cut optimization analysis for vibration control of laminated composite smart structures under uncertainties, App. Math. Mod. 54 (2018) 551–566. https://doi.org/10.1016/j.apm.2017.10.002

[55] V. Fakhari, A. Ohadi, Nonlinear vibration control of functionally graded plate with piezoelectric layers in thermal environment, J. Vib. Cont. 17 (2010) 449–469. https://doi.org/10.1177/1077546309354970

[56] W. Chang, S.V. Gopinathan, V.V. Varadan, V.K. Varadan, Design of robust vibration controller for a smart panel using finite element model, J. Vib. Acoust. 124 (2002) 265-276. https://doi.org/10.1115/1.1448319

[57] J.P. Jiang, D.-X. Li, Optimal placement and decentralized robust vibration control for spacecraft smart solar panel structures, Smart Mater. Struct. 19 (2010) 085020 1-9. https://doi.org/10.1088/0964-1726/19/8/085020

[58] J.P. Jiang, D.-X. Li, Decentralized robust vibration control of smart structures with parameter uncertainties, J. Int. Mat. Sys. Struct. 22 (2011) 137-147. https://doi.org/10.1177/1045389X10391496

[59] K. Zhang, G. Scorletti, M. Ichchou1, F. Mieyeville, Quantitative robust linear parameter varying H_∞ vibration control of flexible structures for saving the control energy, J. Int. Mat. Sys. Struct. 26 (2015) 1006–1027. https://doi.org/10.1177/1045389X14538529

[60] J. Yang, Z. Liu, X. Cui, S. Qu, C. Wang, Z. Lanwei, G. Chen, Experimental study of adaptive sliding mode control for vibration of a flexible rectangular plate, Int, J. Aero. Space Sci. 16 (2015), 28–40. http://dx.doi.org/10.5139/IJASS.2015.16.1.28\

[61] H. Nasser, E.-H. Kiefer-Kamal, H. Hua, S. Belouettar, E. Barkanov, Active vibration damping of composite structures using a nonlinear fuzzy controller, Comp. Struct. 94 (2012) 1385–1390. https://doi.org/10.1016/j.compstruct.2011.11.022

[62] A. Sharma, A. Kumar, C.K. Susheel, R. Kumar, Smart damping of functionally graded nanotube reinforced composite rectangular plates, Comp. Struct. 155 (2016) 29–44. http://dx.doi.org/10.1016/j.compstruct.2016.07.079

[63] J. Wei, Z. Qiu, J. Han, Y. Wang, Experimental comparison research on active vibration control for flexible piezoelectric manipulator using fuzzy controller, J. Intell. Robot. Syst. 59 (2010) 31–56. https://doi.org/10.1007/s10846-009-9390-2

[64] H. Si, D. Li, Active control of vibration using a fuzzy control method based on scaling universes of discourse, Smart Mater. Struct. 16 (2007) 555–560. https://doi.org/10.1088/0964-1726/16/3/001

[65] N.D. Zorić, A.M. Simonović, Z.S. Mitrović, S.N. Stupar, A.M.Obradović, N.S. Lukić, Free vibration control of smart composite beams using particle swarm optimized self-tuning fuzzy logic controller, J. Sound Vib. 333 (2014) 5244–5268. http://dx.doi.org/10.1016/j.jsv.2014.06.001

[66] N. Zorić, A. Simonović, Z. Mitrović, S. Stupar, Active vibration control of smart composite beams using PSO-optimized self-tuning fuzzy logic controller, J. Theor. Appl. Mech. 51 (2013) 275-286. http://www.ptmts.org.pl/jtam/index.php/jtam/article/view/v51n2p275

[67] J. Fu, J. Lai, G. Liao, M. Yu, J. Bai, Genetic algorithm based nonlinear self-tuning fuzzy control for time-varying sinusoidal vibration of a magnetorheological elastomer vibration isolation system, Smart Mater. Struct. 27 (2018) 085010 (1-13). https://doi.org/10.1088/1361-665X/aacd32

[68] J.N. Reddy, On laminated composite plates with integrated sensors and actuators, Eng. Struct. 21 (1999) 568–593. https://doi.org/10.1016/S0141-0296(97)00212-5

[69] T. C. de Godoy, M.A. Trindade, Modeling and analysis of laminate composite plates with embedded active–passive piezoelectric networks, J. Sound Vib. 330 (2011), 194-216. https://doi.org/10.1016/j.jsv.2010.08.010

[70] A. Hac, L. Liu, Sensor and actuator location in motion control of flexible structures, J. Sound Vib. 167 (1993), 239-261. https://doi.org/10.1006/jsvi.1993.1333

[71] Z. Jin, Y. Yang, C.K. Soh, Application of fuzzy GA for optimal vibration control of smart cylindrical shells, Smart Mater. Struct. 14 (2005) 1250-1264. https://doi.org/10.1088/0964-1726/14/6/018

[72] R.M. Jones, Mechanics of Composite Materials, second ed., Taylor & Francis, 1999.

[73] J. Kennedy, R.C. Eberhart. Particle swarm optimization, Proceedings of the IEEE International Conference on Neural Networks, 1995, pp.1942–1948.

Highlights

-Optimization of placement, sizing and orientation of PFRC actuators on smart composite plates
-Analyzis of influence of PFRC fiber orientation on controllability of composite plates
-Active vibration control of smart composite plates using self-tuning fuzzy logic controller
-Optimization of membership functions and output matrices using Particle swarm optimization algorithm